Check for updates

Dayside Aurora

Harald U. Frey[1] (ORCID) **· Desheng Han[2] · Ryuho Kataoka[3,4] · Marc R. Lessard[5] ·
Stephen E. Milan[6,7] · Yukitoshi Nishimura[8] · Robert J. Strangeway[9] · Ying Zou[10,11]**

Abstract Dayside aurora is related to processes in the dayside magnetosphere and especially at the dayside magnetopause. A number of dayside aurora phenomena are driven by reconnection between the solar wind interplanetary magnetic field and the Earth's internal magnetic field at the magnetopause. We summarize the properties and origin of aurora at the cusp foot point, High Latitude Dayside Aurora (HiLDA), Poleward Moving Auroral Forms (PMAFs), aurora related to traveling convection vortices (TCV), and throat aurora. Furthermore we discuss dayside diffuse aurora, morning side diffuse aurora spots, and shock aurora.

✉ H.U. Frey
hfrey@ssl.berkeley.edu

R. Kataoka
kataoka.ryuho@nips.ac.jp

[1] Space Sciences Laboratory, University of California, Berkeley, CA 94720, USA

[2] State Key Laboratory of Marine Geology, School of Ocean and Earth Science, Tongji University, Shanghai, China

[3] National Institute of Polar Research, 10-3 Midori-cho, Tachikawa, Tokyo 190-8518, Japan

[4] Department of Polar Science, SOKENDAI, 10-3 Midori-cho, Tachikawa, Tokyo 190-8518, Japan

[5] Space Science Center, University of New Hampshire, Durham, NH, USA

[6] Department of Physics and Astronomy, University of Leicester, Leicester, UK

[7] Birkeland Centre for Space Sciences, University of Bergen, Bergen, Norway

[8] Department of Electrical and Computer Engineering and Center for Space Physics, Boston University, 725, Commonwealth Avenue, Boston, MA, USA

[9] Department of Earth, Planetary, and Space Sciences, UCLA, Los Angeles, CA, USA

[10] Department of Astronomy and Center for Space Physics, Boston University, Boston, MA, USA

[11] Cooperative Programs for the Advancement of Earth System Science, University Corporation for Atmospheric Research, Boulder, CO, USA

1 Introduction

Aurora is generally considered a nightside phenomenon, primarily because that's where people can easily see it. However, it has been recognized already before the dawn of the space age, that aurora occurs at all local times around the auroral oval, even at local noon (Feldstein 1973). Nightside aurora is related to processes in the magnetotail. Dayside aurora on the other hand is related to processes in the dayside region of the magnetosphere, especially the dayside magnetopause. Therefore it is of particular interest as processes in the dayside magnetosphere are directly related to the solar wind–magnetosphere interaction.

Dayside aurora is difficult to observe from the ground. Because of the offset between the geographic and geomagnetic poles and the distribution of land and oceans there are only very few places on the ground that can actually observe the sky at local magnetic noon, most noticeably on Svalbard and in the Antarctic interior. Furthermore optical observations require darkness which only exists for 1–3 months in local winter. Therefore, dayside aurora optical observations have been rather limited and mostly been done from space where observations in the ultra-violet can separate aurora from the dayglow background.

Many of the localized dayside auroral phenomena have been reviewed in Sandholt et al. (2002a), Frey (2007). All of them occur under specific solar wind conditions and most of them are directly related to magnetic reconnection between the solar wind interplanetary magnetic field (IMF) and the Earth magnetic field at the dayside magnetopause. A summary of the preferred solar wind conditions and the aurora properties are given in Table 1 of Frey (2007) and will not be repeated here. In this paper we will describe a few more dayside auroral phenomena and review the progress in our understanding since 2007.

The vast majority of our discussion will be related to observations in the northern hemisphere. At a few places we will refer to a similar or different behavior in the southern hemisphere.

2 Magnetopause Reconnection

Many dayside auroras are a consequence of magnetic reconnection occurring between the interplanetary magnetic field (IMF) and the terrestrial magnetic field. Reconnection is thought to occur most efficiently where there is a large magnetic shear across the magnetopause. If reconnection occurs where the magnetic shear angle is strictly 180°, then it is referred to as antiparallel reconnection; if the shear angle is less than this, then it is termed component reconnection. The terrestrial field presented to the incoming solar wind is directed northwards at low latitudes and swings around to be directed southwards at high latitudes, pointing towards the northern cusp magnetopause indentation and away from the southern cusp. The orientation of the IMF in the $Y-Z$ plane with respect to the Z-axis, that is its clock angle, θ, is largely preserved as the solar wind traverses the magnetosheath, while the X component is modified by the variable sheath speed so that the sheath magnetic field drapes over the magnetopause. The location and extent on the magnetopause at which reconnection occurs is then largely determined by the clock angle of the IMF and the orientation of the field within. When the IMF is directed southwards ($\theta \approx 180°$) the magnetic

shear is greatest across a large swath of the low latitude magnetopause, where the terrestrial magnetic field lines are closed. For northwards IMF ($\theta \approx 0°$) the magnetic shear is greatest at the high latitude magnetopause, tailward of the cusp openings, where the terrestrial field lines tend to be open and comprise the magnetotail lobes (see Fig. 1). At intermediate clock angles, the two fields are strictly antiparallel in two regions. For $B_Y > 0$, one region starts at the northern cusp and extends southeastwards or northeastwards around the dusk flank if $B_Z < 0$ or $B_Z > 0$; the other extends dawnwards from the southern cusp opening, northwestwards or southwestwards for $B_Z < 0$ or $B_Z > 0$. The dawn and dusk sense of these regions are reversed for $B_Y < 0$. Except for $\theta = 180°$, the antiparallel regions avoid the subsolar magnetopause, such that reconnection at dawn and dusk occurs independently, with ramifications for ionospheric convection patterns (e.g., Coleman et al. 2001). However, there is also considerable evidence that reconnection does occur in the vicinity of the subsolar point when $|\theta| \gtrsim 90°$. It has been proposed, then, that in this clock angle range antiparallel reconnection occurs at the high latitude flanks and component reconnection occurs across a tilted region passing between the antiparallel regions through the subsolar point (e.g., Fuselier et al. 2011). On average the IMF has a Parker spiral configuration with $B_z = 0$, and purely northward and purely southward IMF configurations are rare. Hence Fig. 2(b) and 2(c) are representative of the most common reconnection geometries.

The rate of reconnection, and the steadiness or impulsiveness of reconnection, are then controlled by conditions at the reconnection site. For instance, where the magnetosheath flow is super-Alfvénic steady-state reconnection cannot occur and the interaction is necessarily impulsive. The evolution of newly-opened field lines across the magnetopause, and hence the motion of their footprints in the ionosphere, is controlled by magnetic tension forces and the magnetosheath flow (e.g., Cooling et al. 2001; Fear et al. 2007) and/or by the conductivity (load) of the ionosphere in the hemisphere to which the field line is connected. Many of the influences on the occurrence of reconnection are poorly understood, and are difficult to investigate in situ with spacecraft due to the vastness and sporadic motions of the magnetopause. Much, however, can be gleaned from a study of the convective ionospheric motions excited by reconnection and the associated auroras created by particles injected from the magnetosheath on newly-opened field lines. Understanding magnetopause reconnection is a major motivation for studying the dayside auroras.

3 Ionospheric Convection

Magnetic reconnection at the magnetopause and in the magnetotail drives a circulation of plasma within the magnetosphere, which determines the general structure of the magnetosphere and the morphology and dynamics of the auroras. This circulation is most easily monitored in the ionosphere, using e.g. the Super Dual Auroral Radar Network (Super-DARN) (Chisham et al. 2007). The behaviour of this circulation depends mainly on the north/south orientation of the IMF (see Fig. 1).

When the IMF is directed southwards, reconnection occurs across a broad region of the dayside magnetopause, opening previously closed field lines (Fig. 1a). This leads to an antisunwards ionospheric convection in the dayside polar cap, but a sunwards (equatorwards) motion of the dayside polar cap boundary (PCB) and the dayside auroras as the open magnetic flux content of the magnetosphere increases (Cowley and Lockwood 1992). This represents the loading due to the expansion of the polar cap and lobe pressure increase and is often referred to as substorm growth phase. Periods of southwards IMF are usually followed by the onset of magnetic reconnection in the magnetotail, substorm expansion phase
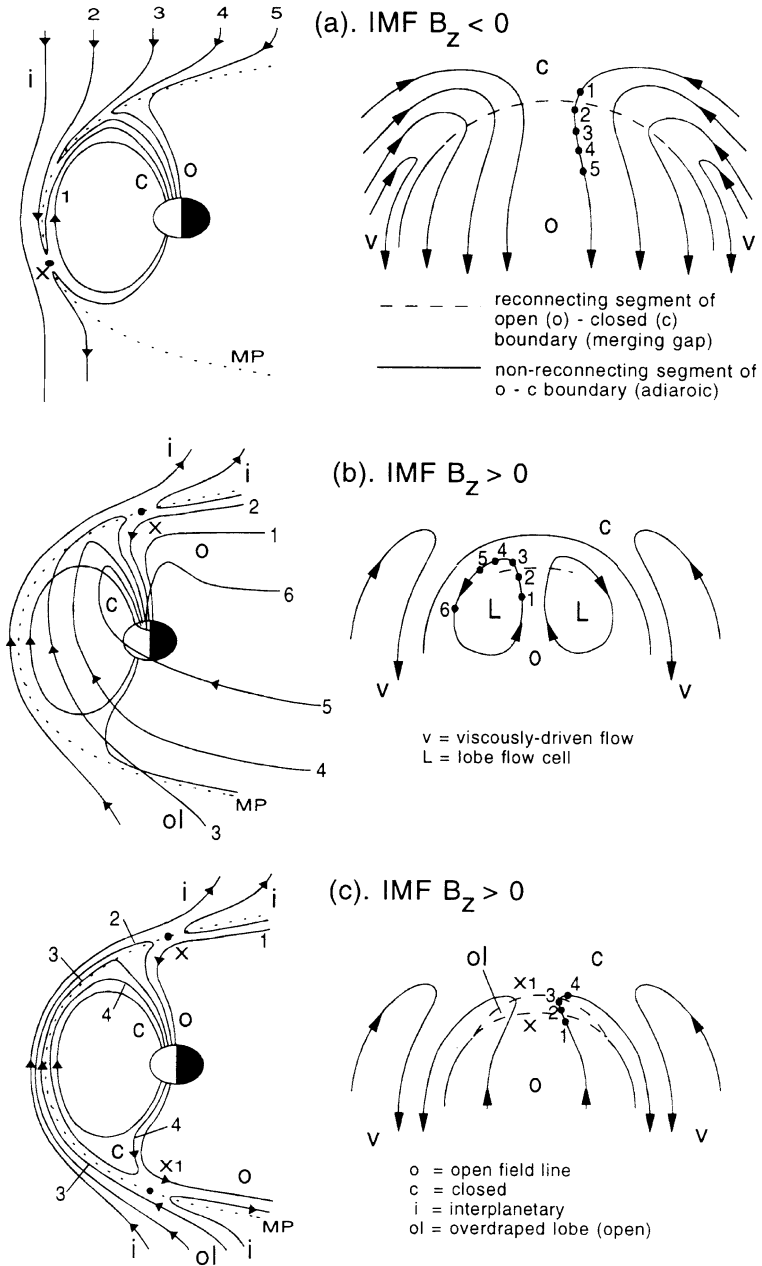
Fig. 1 Schematic illustrations of (left) the evolution of reconnected field lines in the magnetosphere, as seen from the dusk flank and (right) the corresponding flow in the northern hemisphere ionosphere for magnetopause reconnection during (**a**) southward IMF and (**b** and **c**) northward IMF, with $B_y \approx 0$. Field lines and regions that are open, closed, interplanetary and overdraped lobe are labelled, respectively, o, c, i, and ol. From Lockwood ([1998](#))
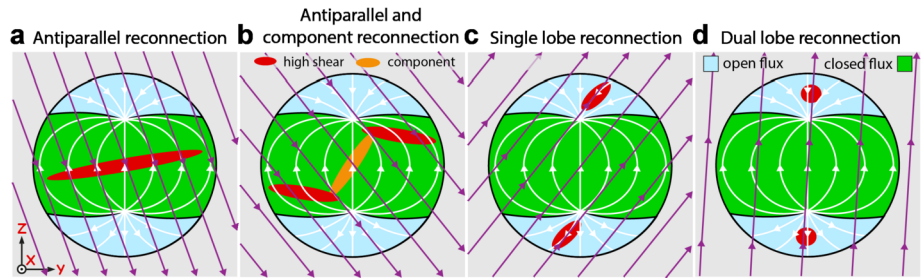
Fig. 2 Four panels showing possible reconnection geometries for different orientations of the IMF. (**a**) Clock angle near 180°, where antiparallel reconnection occurs across the dayside magnetopause at low latitudes. (**b**) Clock angle near 135°, where antiparallel reconnection occurs away from the equatorial plane and component reconnection occurs near the subsolar point. (**c**) Clock angle near 45°, where antiparallel reconnection occurs tailwards of the cusps, but with different IMF field lines in the two hemispheres. (**d**) Clock angle near 0°, where antiparallel reconnection occurs tailwards of the cusps, but with the same IMF field line in the two hemispheres

onset, to reduce the open flux content of the magnetosphere, and a cyclical expansion and contraction of the polar cap can ensue (Milan et al. 2003, 2007), leading to polewards and equatorwards motions of the dayside auroras. Within the dayside polar cap, the B_Y component of the IMF leads to a dawn-dusk asymmetry in the flows, with a dawnward (duskward) sense to the flows for $B_Y > 0$ ($B_Y < 0$) in the northern hemisphere (and opposite in the southern hemisphere).

For northwards IMF, reconnection occurs with the open field lines of the lobes, producing sunwards convection in the dayside polar cap. Single-lobe reconnection, when reconnection occurs independently in each hemisphere (Fig. 1b), leads to twin-reverse convection cells contained entirely within the polar cap; the relative size of the two cells depends on the polarity of IMF B_y, producing a larger pre-noon (post-noon) cell for $B_Y > 0$ in the northern (southern) hemisphere. Dual-lobe reconnection (Fig. 1c) closes open flux and sunward convection occurs across the dayside polar cap boundary as the polar cap contracts (e.g., Imber et al. 2006).

The transmission of stress from the magnetopause and magnetosphere to the ionosphere to cause convection is accomplished by electrical currents that flow along magnetic field lines into and out of the ionosphere. Upwards electrical currents are carried by downwards-precipitating electrons, often producing auroras. The large-scale auroral morphology is determined by the configuration of these currents (e.g. Milan et al. 2017), and the dayside auroras reviewed in this paper sit within this overall context.

4 Source Regions for Auroral Particles

The ionospheric regions where dayside aurora occurs map along magnetic field lines to the dayside region of the magnetosphere. Many years of particle measurements were used to infer the magnetospheric source region from the general energy spectral properties of precipitating electrons (Newell et al. 2005) and ions (Newell et al. 2009). Figure 3 shows the distribution in magnetic latitude and local time for the different inferred source regions for varying solar wind conditions. As Newell et al. (2005) point out these maps are averages and on a particular day or time a specific auroral precipitation region can show up at a different location. But these maps provide an excellent basis for the identification of the most likely

Precipitation Regions
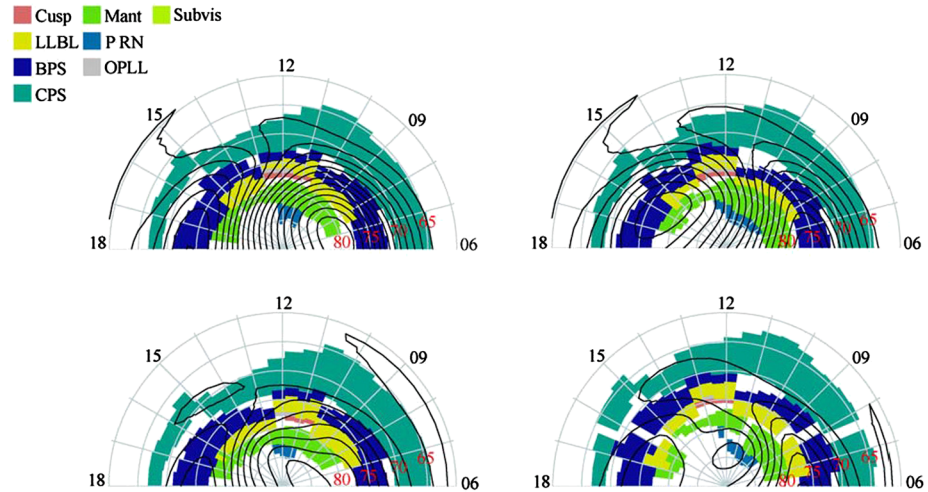
Fig. 3 A map of the dayside precipitation regions binned by interplanetary magnetic field (IMF). Top left, $B_z < -1$ nT, $B_y < -3$ nT; top right, $B_z < -1$ nT, $B_y > 3$ nT. Bottom left, $B_z > 1$ nT, $B_y < -3$ nT. Bottom right, $B_z > 1$ nT, $B_y > 3$ nT. ("OPLL" refers to open low-latitude boundary layer; "P RN" refers to polar rain; "LLBL" refers to Low Latitude Boundary Layer; "BPS" refers to Boundary Plasma Sheet; "CPS" refers to Central Plasma Sheet). From Newell et al. (2005)

source region of auroral particles if in situ measurements are not available (Newell et al. 2004). Furthermore, the investigations determine the average probability of electron acceleration and energy flux coming from these inferred source regions. The highest probability for electron acceleration events comes from the boundary plasma sheet (BPS), followed by the cusp and the Low Latitude Boundary Layer (LLBL) just equatorward of the cusp.

Electron acceleration in the cusp is surprisingly low. Even though acceleration events are often observed in the cusp, their typical energy is usually less than a few hundred electron-volts. Electron acceleration events are quite common in the LLBL, their average energy can exceed many hundreds of electronvolts. Newell et al. (2005) speculate that the higher energy makes the related aurora easily visible from ground-based optical observation sites.

As a general result Newell et al. (2005) find that the regions lying further equatorward, and particularly on closed field lines, have accelerated electrons with higher associated energy fluxes and thus show aurora more frequently. The post-noon LLBL and, especially, the post-noon BPS have the highest number of events and the largest associated energy fluxes. The peak energy of precipitation also rises moving equatorward, with the exception that the events occurring within the cusp and open LLBL have even lower average energy than those in the mantle.

5 Aurora Related to Dayside Reconnection

The majority of dayside aurora are related to dayside reconnection (see Sect. 2). In this section we will review those phenomena that are created by or related to dayside reconnection while later sections will summarize phenomena that are related to other processes.
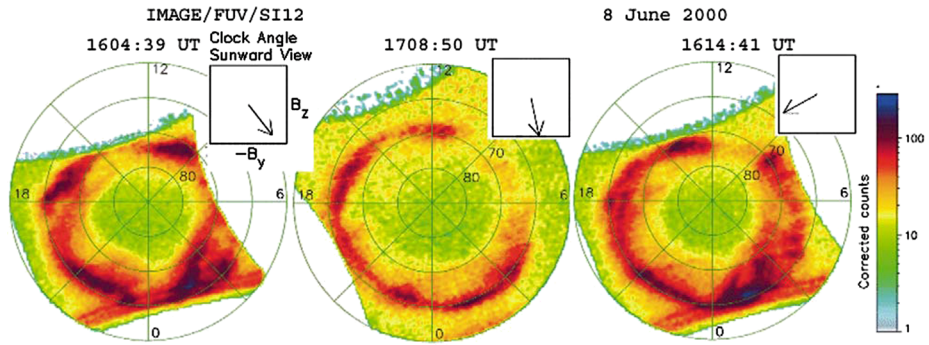
Fig. 4 Three images during a southward IMF interval showing that the cusp footpoint moves as the IMF B_y changes. The clock angles are shown as viewed from the Earth. The cusp is located on the dawnside (duskside) of the auroral oval when the IMF B_y is negative (positive). From Fuselier et al. (2003)

5.1 Cusp Aurora During Southward IMF

As discussed in Sect. 3, during southwards IMF, the opening of closed field lines at the magnetopause leads to poleward convection across the dayside polar cap boundary (PCB). Equatorwards of the PCB, auroral emission is dominated by diffuse green line aurora at 557.7 nm (see also Sect. 7), produced by trapped, hot magnetospheric plasma. Polewards of the PCB, the auroras are dominated by red line 630.0 nm emissions produced by precipitation of cool magnetosheath plasma, injected along newly-opened field lines (e.g., Lockwood et al. 1993; Lockwood 1997).

The time-of-flight of magnetosheath ions from the magnetopause to the ionosphere depends on their energy, leading to a latitudinal energy dispersion on the poleward-convecting field lines (e.g., Reiff et al. 1977; Woch and Lundin 1992; Trattner et al. 2002). Discontinuities in the energy-dispersion, leading to a "staircase" appearance are linked to non-steady reconnection at the magnetopause (e.g., Newell and Meng 1991; Lockwood et al. 1998). Such signatures have been observed in conjunction with poleward convection and quasi-period poleward-moving auroral forms (PMAFs) (e.g., Yeoman et al. 1997; Lockwood et al. 2001a). A similar association has been drawn between pulsed bipolar magnetic field signatures at the magnetopause, known as flux transfer events (FTEs) and also interpreted as a result of transient reconnection, and pulsed ionospheric flows and radar auroras (e.g., Neudegg et al. 2000; Wild et al. 2001). The study of PMAFs has since focused on understanding the role of transient reconnection in solar wind-magnetosphere coupling, which occurs even during periods of steady southwards IMF (see Sect. 5.4 for more details).

In global space-based views the cusp aurora during southward IMF appears as a brighter latitudinally thin and longitudinally extended region (Frey et al. 2003b) that is merged with the poleward part of the dimmer dayside diffuse aurora (Fig. 4). The local time location changes with the IMF B_y as the reconnection site at the low latitude dayside magnetopause moves in longitude. Magnetic mapping confirmed this connection (Frey 2007). The relative displacement in magnetic latitude in response to changes in the magnitude of the IMF B_z will be discussed in Sect. 5.2.

5.2 Cusp Aurora During Northward IMF

During northward IMF the reconnection site at the dayside magnetopause moves to the high latitude lobes (see Fig. 1). The cusp foot point moves to higher latitudes and gets clearly

separated from the dayside auroral oval. As a result, global images show a clear cusp spot (e.g., Milan et al. 2000b) which has been extensively studied using IMAGE FUV proton aurora images (see e.g. Frey et al. 2002, 2003c; Fuselier et al. 2002; Frey 2007).

Earlier studies from the ground already revealed many of the general properties of cusp aurora and its dependence on the IMF B_z, B_y and solar wind dynamic pressure (see Sandholt et al. 2002a for event studies and references within). Even though ground-based observations can often detect small-scale features of the cusp aurora it also has to be realized that the limited coverage occasionally can lead to wrong conclusions about the disappearance of aurora which in reality just moved outside of the observation region. Furthermore, these observations are limited to just a few weeks of dark skies around local winter solstice. The main properties of cusp aurora during northward IMF and in the northern hemisphere can be summarized as follows (Sandholt et al. 2002a):

1. Strong emission both in 557.7 nm and 630.0 nm
2. Occurrence generally within the 0900-1500 MLT and 75°–80° MLAT region
3. Postnoon and prenoon occurrence depending on positive/negative IMF B_y
4. B_y dependent east-west motion of brightening events
5. Short term variability of brightness with stepwise poleward expansions followed by equatorward retreat
6. Decreasing brightness towards background when the IMF rotates from northward to a radial orientation

The proton aurora channel of the IMAGE FUV instrument allowed for extended studies of cusp aurora dynamics on the one hand because of the nonexistent background even during full solar illumination of the cusp foot point. On the other hand, the long orbital period of the satellite allowed for extended times of uninterrupted observations. The early studies established the strong relationship between the solar wind dynamic pressure and the cusp aurora brightness and confirmed particle measurements that ion precipitation can provide up to 60% of the total energy flux into the cusp (Frey et al. 2002; Østgaard et al. 2005).

Magnetic field line mapping with modern geomagnetic field models is much more reliable on the dayside than on the nightside because the dayside magnetosphere is compressed by the solar wind and much more stable than on the nightside where field lines can get substantially stretched. That allowed in several cases the mapping either from a spacecraft down to the cusp foot point, or from the cusp aurora out into the magnetosphere and to the magnetopause. When the Cluster spacecraft crossed the magnetopause and observed diverging proton jets from antiparallel reconnection at the high-latitude magnetopause the proton aurora imager observed a bright aurora spot (Phan et al. 2003). The field line mapping connected the satellite at the magnetopause during the jet observations with the bright cusp aurora spot and provided the direct evidence for their relationship.

Long periods of steady northward IMF provided unprecedented opportunities for the investigation of the steadiness of reconnection and cusp proton aurora generation (Frey et al. 2003c). Figure 5 shows examples of mapped proton aurora observations during one of these occasions where the inserts of the IMF orientation track the prenoon and postnoon motion of the proton aurora spot remarkable well. The IMAGE SI-12 channel had an imaging cadence of one image every two minutes. Therefore, nothing can be said about shorter period fluctuations. However, the continued presence of the proton aurora spot for many hours allowed (Frey et al. 2003c) to conclude that reconnection for northward IMF is a directly driven process that never stops on a global scale but is continuous and quasi-steady for as long as the driving solar wind conditions do not change substantially.

The mapping of the cusp aurora was used to estimate the length of the reconnection line at the magnetopause. During southward IMF a much longer X-line of 10–25 R_e was
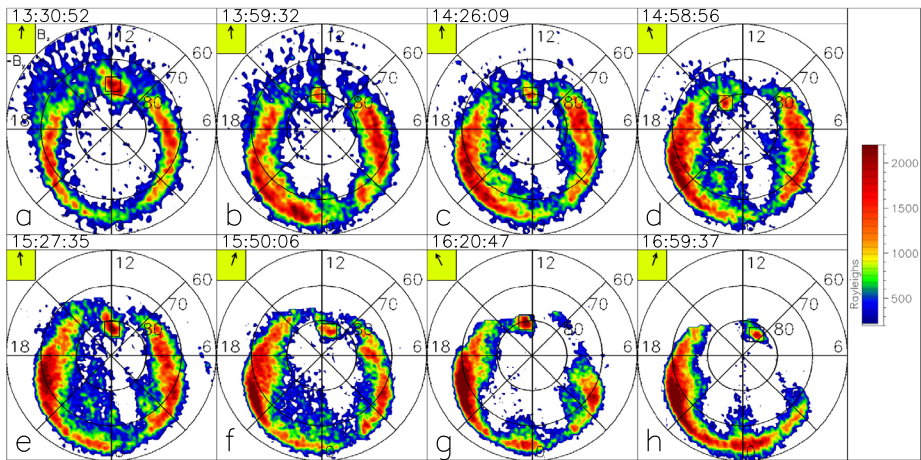
Fig. 5 Snapshots of the proton aurora oval and spot on 18 March 2002 showing the continuous presence of the proton aurora spot. The Spectrographic Imager channel SI-12 on board the IMAGE spacecraft observes Doppler-shifted Lyman-α emission from precipitating protons with energy of several keV. The images are shown in a geomagnetic grid of latitudes and local time with the noon meridian at the top and morning 06:00 h pointing to the right. The solar-wind magnetic field in the y–z GSM plane is shown in the upper left insert, with north ($B_z > 0$) pointing up and east ($B_y > 0$) pointing to the left. The black square in each panel covers the 500×500 km^2 area around the spot. The dayside proton aurora spot is seen uninterruptedly over ~4 hours. The spot appears on the dayside at ~80° latitude. Its location in magnetic local time (MLT) is correlated with the y-component of the solar-wind magnetic field, being in the pre-noon (post-noon) sector for negative (positive) B_y. From Frey et al. (2003c)

determined compared to the much shorter estimate of 3–5 R_e for northward IMF (Fuselier et al. 2002). The longer X-line for southward IMF explains the larger size and brightness of the cusp aurora during southward IMF compared to northward conditions and is consistent with measurements of much larger ion number fluxes (Frey 2007).

One remarkable similarity between cusp aurora during northward and southward IMF is their MLT location dependence on the IMF B_y. Positive and negative IMF B_y move the cusp foot point, and the corresponding reconnection site at the magnetopause, to later and earlier local time, respectively. During northward IMF the dependence is:

$$MLT = 11.8 \text{ hours} + 0.127 * B_y \tag{1}$$

While during southward IMF a dependence of

$$MLT = 12.6 \text{ hours} + 0.120 * B_y \tag{2}$$

Was determined (Frey et al. 2002, 2003b).

The cusp footpoint moves in magnetic latitude during southward IMF. Observation with the TIMED-GUVI instrument provided a linear relationship of 1.1° change in magnetic latitude for each Nano-Tesla of southward IMF (Zhang et al. 2005). For northward IMF no such relationship could be found indicating that the reconnection site under these conditions must be quite fixed at the high latitude lobe while during southward IMF the reconnection region can move much more freely along the dayside magnetopause (Frey et al. 2002). These results from aurora observations are in very good agreement with cusp modeling and observations which found the following relationships for the Cusp equatorward boundary

(Ceb; Wing et al. 2005):

$$Ceb = (0.81 \pm 0.05) IMF B_z + (77.7 \pm 0.2)° \text{ for southward IMF and} \qquad (3)$$

$$Ceb = (0.04 \pm 0.06) IMF B_z + (78.1 \pm 0.2)° \text{ for northward IMF} \qquad (4)$$

Other relationships of the equatorward and poleward cusp boundaries with respect to the IMF B_z and other solar wind coupling functions can be found in Newell et al. (2006), Johnsen and Lorentzen (2012).

The operation of the Polar UVI in the south and IMAGE FUV instrument in the north allowed for observations to confirm the simultaneous presence of the cusp aurora in both hemispheres. Reconnection during northward IMF should occur at both high latitude lobes and the cusp spots should be visible. The cusp spots were found at different local times (1000–1200 MLT in the north and 1200–1700 in the south) which is to be expected as a response to opposite IMF B_y control (Østgaard et al. 2005). The difference in latitude between the hemispheres was explained with the dipole tilt angle that shifted the reconnection site in the south to higher latitudes compared to the north.

5.3 High Latitude Dayside Aurora (HiLDA)

Few reports had been published about an aurora at dayside high latitudes before observations by the IMAGE FUV instrument allowed for a more detailed and systematic study of this phenomenon (Frey et al. 2003a). A very localized aurora could be seen in UV images of an otherwise empty polar cap which could last for many hours during otherwise quiet geomagnetic conditions. The absence of a signature in the proton aurora and a few in situ measurements by low altitude satellites (Fig. 6) confirmed their generation by pure high energy electron precipitation (Frey et al. 2003a). Field lines from this High Latitude Dayside Aurora (HiLDA) mapped very far into the tail while field lines from a simultaneously observed northward IMF cusp footprint (see Sect. 5.2) mapped to the high latitude magnetopause confirming the occurrence of reconnection but pointing to potentially lobe reconnection for the HiLDA spot. Very distinct external conditions for the HiLDA occurrence were northward IMF B_z, a strong dominating positive IMF B_y, very low solar wind density, and northern summer (Frey et al. 2004).

Model calculations of the ionospheric convection with these external conditions put the cusp aurora at the foot point of a downward field-aligned current in the center of a convection cell at the dayside. The HiLDA spot is in the center of the dominating clockwise convection cell with upward field-aligned current. These observational and modeling results then led to an explanation of the HiLDA occurrence as the result of a multi-step process. The northward B_y dominated IMF drives high latitude reconnection with a downward current into the cusp. Ionospheric convection drives the upward current over the HiLDA and both currents are connected by Pedersen currents in the high-conductivity sunlit summer ionosphere. The drop of the solar wind density before the HiLDA occurrence reduces the number of available current carriers (electrons) in the upward field-aligned current leg and the system sets up an accelerating potential in order to drive more of the available electrons into the loss cone to keep the current going. In astrophysics this process is called 'current starvation' (Kuijpers et al. 2015).

Conjugate observations in both hemispheres were used to study the asymmetric response of geospace to a strong IMF B_y driving during a geomagnetic storm (Østgaard et al. 2018). The strong IMF combined with a large dipole tilt led not only to large asymmetries in the
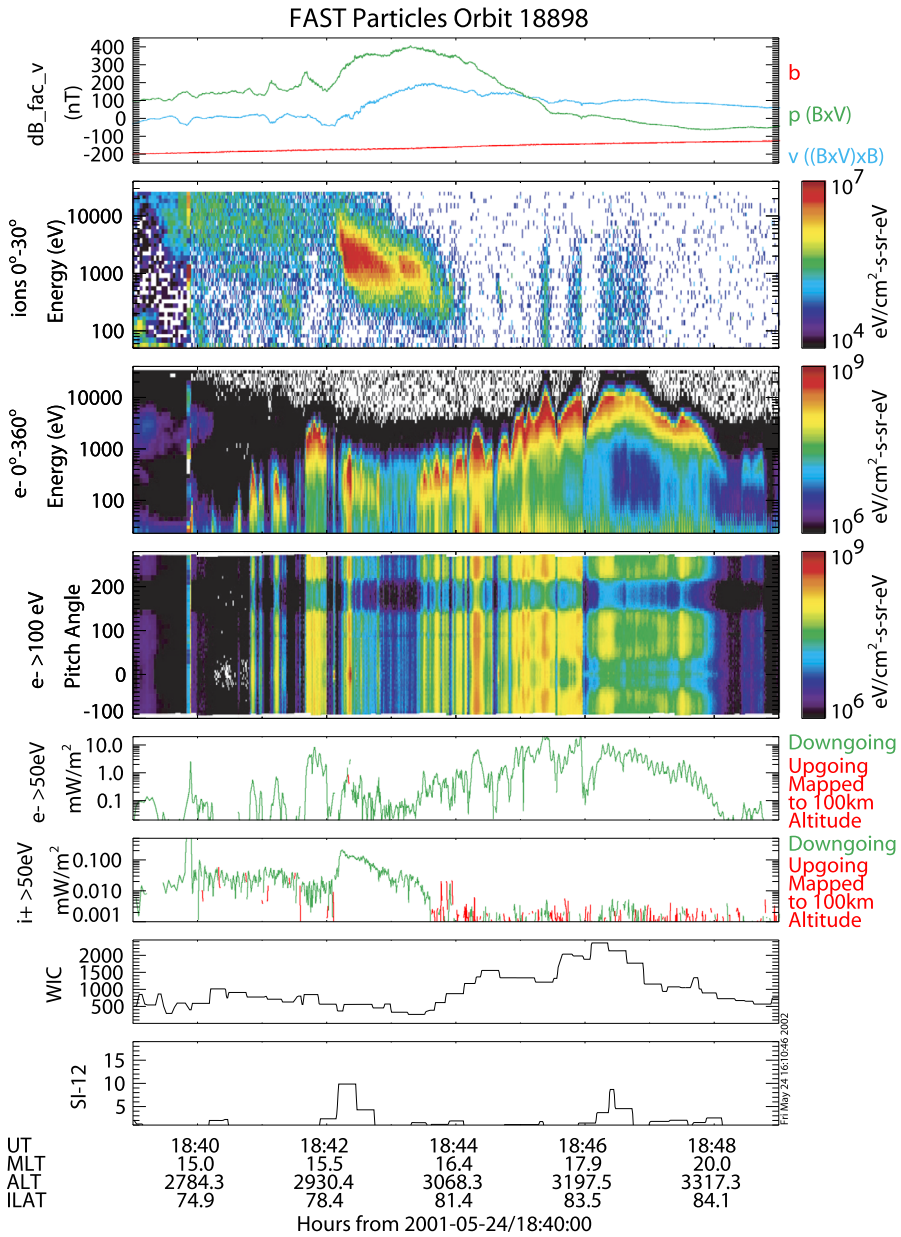
Fig. 6 FAST measurements and FUV observations of a HiLDA spot. The background IGRF magnetic field was subtracted from the FAST magnetic field measurements and the top panel shows the three components of the remaining magnetic field disturbance along the background field (red), perpendicular to the background field and the spacecraft velocity vector (green) and along the spacecraft track (blue). The green line represents the magnetic field disturbance that is created by field-aligned currents with a positive (negative) slope for a downward (upward) current. The next panel is the ion energy spectrogram in the loss cone. Then follow the electron energy spectrogram and the pitch angle distribution. The next two panels summarize the energy fluxes of electrons and ions, mapped to 100 km altitude. The last two panels are the count rates in the six consecutive electron and proton aurora images along the footprint of FAST (reproduced from Frey et al. 2003a)

dawn and dusk auroral ovals but also to the occurrence of the HiLDA spot only in the northern hemisphere, but not in the south. These observations were interpreted as a strong signature that lobe reconnection only occurred in the northern summer hemisphere.

Based on the distinct external conditions for HiLDA in the northern hemisphere Frey (2007) predicted a similar occurrence during summer in the southern hemisphere with negative IMF B_y and positive B_x. These predictions were recently confirmed by Carter et al. (2018) who used a large database of auroral observations and field-aligned current measurements. They found bright HiLDA spots only during southern summer with the predicted IMF orientation confirming the IMF-magnetosphere electrodynamic coupling that creates this particular localized aurora.

### 5.4 Poleward Moving Auroral Forms (PMAFs)

Dayside discrete aurora often shows a repetitive poleward motion of auroral arcs. It was first documented in the 1970's (Vorobjev et al. 1975; Horwitz and Akasofu 1977), and was recognized as an ionospheric signature of transient reconnection along the dayside magnetopause. This type of aurora, later referred to as poleward moving auroral forms (PMAFs) (Fasel et al. 1993), is characterized by brightening near the equatorward boundary of dayside discrete aurora (equatorward boundary intensification or EBI), followed by poleward motion. This sequence manifests an ionospheric signature of flux transfer events (FTEs, see below for more details) (Sandholt et al. 1986).

Early observations of PMAFs were made with meridian scanning photometers (e.g., Sandholt and Newell 1992), showing that these features were embedded within red line auroras and hence were probably associated with newly-opened field lines. Milan et al. (1999a, 1999b) demonstrated a close association between PMAFs and poleward bursts of convective flow. In addition, a sawtooth motion of the PCB was observed during its general equatorward progression, which suggested periodic erosion of closed flux associated with each burst of reconnection. Still to be resolved, however, is why individual PMAFs are latitudinally separated by regions devoid of auroras: each new region of open flux should be spatially contiguous, and hence no "gap" is expected in the auroral emission. Lockwood et al. (2001a) speculated that the auroral forms were produced by field-aligned currents at the boundaries between adjacent regions of newly-opened flux, associated with convection shears driven by differential azimuthal tension forces associated with IMF B_Y; however, no subsequent studies have followed up on this suggestion.

Figure 7 shows a typical event that presents a series of PMAFs after an IMF southward turning. Figure 8 schematically illustrates the PMAF sequence and the relation to large-scale precipitation and convection. Each PMAF starts with an EBI and then propagates poleward. The equatorward boundary of the 630.0 nm wavelength aurora overall moves equatorward as expected from enhanced magnetopause reconnection under the southward IMF. Note that the equatorward motion is not monotonic but stepwise, where the boundary rapidly shifts equatorward by $\sim 0.5°$ magnetic latitude (MLAT) with each EBI initiation and then slows down or slightly retreats poleward (Horwitz and Akasofu 1977; Pudovkin et al. 1992). This boundary motion indicates a transient enhancement and then reduction of magnetopause reconnection associated with each PMAF.

Each PMAF is oriented approximately azimuthally (~ 500 km east-west and ~ 50 km north-south). As Figs. 7c–h show, the equatorward boundary motion associated with the EBIs is also localized, indicating that the enhanced magnetopause reconnection is localized azimuthally. PMAFs have a lifetime and recurrence period of $< \sim 10$ min (Fasel 1995) and a poleward propagation speed of ~ 1 km/s (Oksavik et al. 2005). PMAFs can also extend over
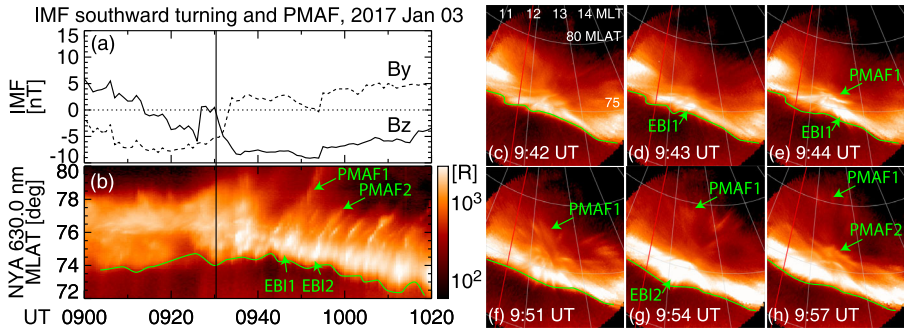
Fig. 7 A series of PMAFs associated with IMF southward turning, measured by the Ny-Alesund (NYA) all-sky imager at Svalbard on 3 January 2017. (**a**) IMF B_y and B_z, (**b**) 630.0 nm wavelength keogram, and (**c–h**) the sequence of two of the PMAFs. The green curve traces the 1 kR contour as a proxy of the open-closed boundary. The red line in Panels (**c–h**) shows the magnetic noon

Fig. 8 Schematic illustration of PMAF and related processes in the dayside auroral oval under a typical IMF condition for PMAF occurrence ($B_z < 0$ and $B_y > 0$). The gray lines depict poleward propagation of the EBI-PMAF-patch sequence
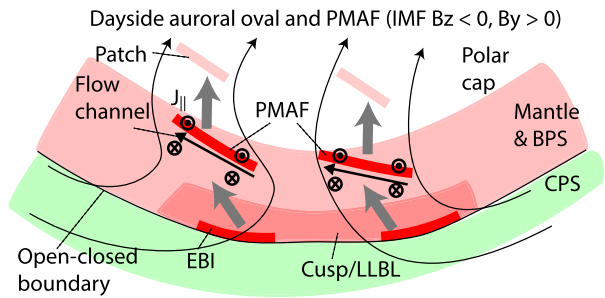
much larger east-west size (>7 h MLT extent) and the azimuthal size has been suggested to be controlled by the solar wind speed (Milan et al. 2016).

PMAFs are generally a phenomenon under southward IMF. A typical example is shown in Fig. 7. Initially the dayside discrete aurora stays at higher latitudes without PMAFs under northward IMF, and when an IMF southward turning occurs, the pre-existing discrete aurora fades and a new discrete auroral activity emerges equatorward of the pre-existing aurora and a series of PMAFs occurs as the discrete aurora overall moves equatorward (Sandholt and Farrugia 2002). However, while more than half (∼60%) of PMAFs occurs under southward IMF, it is nevertheless not uncommon to have PMAFs under northward IMF (Fasel 1995; Drury et al. 2003; Xing et al. 2012). The PMAF occurrence and location are rather strongly controlled by IMF B_y, where PMAFs are more frequent under positive IMF B_y in the northern hemisphere at post-noon (negative B_y at pre-noon in the southern hemisphere) (Sandholt et al. 2004). PMAFs under negative IMF B_y occur at pre-noon, and the occurrence rate near noon is smaller than pre- and post-noon (midday gap) (Fasel 1995; Sandholt et al. 2004). PMAFs are most often found at $|B_y|/|B_z| \geq 1 (B_z < 0)$, while aurora under $|B_y|/|B_z| < 1 (B_z < 0)$ is characterized as a quasi-steady longitudinally extended band at lower intensity with fewer PMAFs. A majority of PMAFs rebrighten during poleward propagation (Fasel 1995). The rebrightening time scale (a few minutes) is comparable to the Alfvén transit time and is considered to be due to a sequence of Alfvén waves launched from the reconnection region.

PMAFs under positive IMF B_y propagate dawnward (Fig. 8), and PMAFs under negative IMF B_y propagate duskward. The IMF B_y dependence is consistent with the release of magnetic stress of the reconnected field lines between the IMF and dayside magnetosphere. The azimuthal motion of PMAFs can be considerably large, giving rise to PMAFs moving ∼3–5 h MLT away from noon (Wang et al. 2016a).

PMAFs do not necessarily occur only at a single location in the dayside auroral oval but can occur at more than one location. During time intervals of IMF $|B_y|/|B_z| \geq 1 (B_z < 0)$, PMAFs are found both at pre-noon and post-noon with a gap at noon (see Fig. 8 for $B_y > 0$), while PMAFs in different regions are not synchronized (Sandholt et al. 2003a; Maynard et al. 2006). This structure is interpreted as activation of magnetopause reconnection at multiple sites.

It is important to identify whether PMAFs are triggered by solar wind parameter changes or occur spontaneously. Both types of events have been reported. PMAFs can occur in association with IMF orientation or solar wind dynamic pressure changes (Sandholt et al. 2003b; Maynard et al. 2006; Mende et al. 2009). PMAFs can also occur under quasi-steady solar wind (Sandholt and Farrugia 2002; Sandholt et al. 2003b). Until recently, there was no systematic study of how often PMAFs are triggered or occur spontaneously. In addition, solar wind observations far from the subsolar bow shock have been used in past studies, which are problematic for estimating actual solar wind conditions reaching the bow shock. The solar wind could evolve during the propagation or the solar wind may contain smaller-scale structures that may miss the satellite location but reach the bow shock. To address these issues, Wang et al. (2016b) used the THEMIS outer probes-all sky imager conjunctions and found that 70% of PMAFs are preceded by IMF orientation changes, indicating that a majority of PMAFs are triggered by solar wind parameter changes. The IMF at the THEMIS outer probes are markedly different from OMNI data; the IMF southward turnings seen at THEMIS do not always exist in OMNI. This means that IMF evolution or localized structures are important for accurately understanding dayside magnetospheric responses.

PMAFs are part of a dynamical and localized magnetosphere-ionosphere coupling system that involves a localized flow channel and current system (Fig. 8). Localized field-aligned currents (FACs) have been detected in association with PMAFs and flow channels (Sandholt and Newell 1992), and the FACs and horizontal currents create poleward moving magnetic field perturbations on the ground (Milan et al. 2000a). PMAFs lie along the flank of the flows where the velocity shear is clockwise when viewing from above (Oksavik et al. 2004, 2005), as expected from the relation between FACs and flow shears.

Precipitating particle measurements show that PMAFs are associated with enhanced electron precipitation of hundreds of eV (Oksavik et al. 2005; Lorentzen et al. 2010). Electron precipitation creates substantially enhanced density, electron heating and ion upflow in the F-region ionosphere, while ion temperature responses depend on the location relative to the cusp (Lockwood et al. 2000; Skjaveland et al. 2011). Joule heating is also enhanced during PMAFs and is estimated to consume a tenth of the solar wind energy that has entered the magnetopause reconnection region (Pudovkin et al. 1992).

As mentioned above, PMAFs occur in association with flows of enhanced velocities ($> \sim 1$ km/s) that are superimposed on the cusp convection (Thorolfsson et al. 2000; Neudegg et al. 2001). These flows are important as they reflect the momentum transport aspect of FTEs. Depending on their exact characteristics, and the parameter in which they are identified, the flows are named as flow/convection channels, flow bursts, pulsed ionospheric flows, or poleward moving radar auroral forms (PMRAFs) (see Wild et al. 2001; Davies et al. 2000). The differently named flows are very much related, and in some cases describe the same phenomena (Davies et al. 2000). Moen et al. (2012) have summarized four representative types of flow channels.

Similarly to the PMAF optical properties, the enhanced flows generally occur in the pre-noon (post-noon) sector when the IMF By is positive (negative) (Provan et al. 1999). They are not limited to southward IMF conditions but can occur during prolonged northward IMF intervals (Provan et al. 2005). They occur repetitively on time scales of minutes to a few tens of minutes and the repetition rate may be associated with fluctuations in the solar wind (Prikryl et al. 2002; Rae et al. 2004). While statistically the flow occurrence rate appears to decrease with increasing repetition period (McWilliams et al. 2000a), the distribution is fitted well with a power-law-like power spectrum, implying no actual preferred timescale (Abel and Freeman 2002). The flows vary broadly in size from tens to thousands of km (Provan and Yeoman 1999; Oksavik et al. 2005) and factors controlling the size are not clearly understood. The flows contribute significantly to plasma transport with a potential drop of a few to tens of kV, which is often a few tenths of the total transpolar potential drop (Lockwood et al. 1990; Glassmeier and Stellmacher 1996).

Observations also reveal a new category of cusp flows that are directed oppositely to the background convection, termed as reversed flow events (RFEs) (Rinne et al. 2007). While they were initially interpreted as return flows of the increased anti-sunward flows, they are later noticed not to always follow the propagation of PMAFs but associate with Birkeland current arcs moving with the cusp/cleft boundary (Moen et al. 2008). The exact driver has not yet been clearly resolved.

The magnetospheric driver of PMAFs is identified as FTEs, products of time varying magnetopause reconnection (Haerendel et al. 1978; Russell and Elphic 1979), or solar wind dynamic pressure pulses. The former is a more common driver than the latter (Xing et al. 2012). After formation, FTEs propagate anti-sunward away from the X-line where they can be identified through their characteristic bipolar magnetic field perturbations normal to the magnetopause and mixed plasma populations of magnetospheric and magnetosheath origin (Paschmann et al. 1982; Farrugia et al. 1988). Southwood (1987) predicts that FTEs connect to the ionosphere via a pair of FACs and that the upward FAC illuminates as auroral transients. The FACs also transfer momentum of FTEs down to the ionosphere, inducing the flows of enhanced velocities that have been discussed above. This model is supported by numerous space-ground coordinated observations (Moen et al. 2012; Carlson 2012).

A key question regarding transient reconnection is the length of the reconnection X-line on the magnetopause, the extent of the PCB over which the associated PMAF extends, and hence the contribution to the total reconnection voltage (e.g., Lockwood et al. 1995). Many early studies of PMAFs were undertaken with ground-based cameras with a limited field-of-view, which lead to an underestimate of the open magnetic flux in each FTE ($<1\%$ of the pre-existing polar cap flux) and hence the contribution of FTEs to convection. Space-based auroral imagery of PMAFs revealed that coherent auroral features could occupy up to 7 hours of MLT around the boundary and contain up to 10% of the polar cap flux, sufficient to represent the total voltage associated with the growing polar cap (e.g., Milan et al. 2000a). Moreover, these features began their poleward progression first near noon and then at later local times, suggesting a reconnection X-line that grew from the subsolar point around the flank of the magnetopause, a suggestion first proposed by Lockwood et al. (1995). More recent studies have confirmed that such FTEs are a common occurrence, and have allowed the magnetopause structure of FTEs to be explored (e.g., Fear et al. 2017). There are still, however, significant questions regarding why reconnection is pulsed, the exact relationship between FTEs at the magnetopause and their auroral signatures in the ionosphere, and what controls the local time extent of the reconnection X-line (e.g., Milan et al. 2016).

Case studies show that FTEs and the enhanced flows are one-to-one related (Wild et al. 2003; Marchaudon et al. 2004) and that the shape, east-west extent, and drift velocity of

FTEs are consistent with those of the flows (Lockwood et al. 2001a,b). The motion of FTEs agrees with the motion of PMAFs (Zhang et al. 2010). A fortuitous event even captures Alfvén waves carrying FACs down the reconnected flux tubes to the enhanced flows (Farrugia et al. 2004). Statistically, 77% of FTEs are associated with the enhanced flows, and 64% of the enhanced flows are associated with FTEs (Neudegg et al. 2000).

PMAFs and related ionospheric enhanced flows have been advantageous in uncovering the macroscopic properties of FTEs that are not easily accessible from the spacecraft point measurements alone. For example, Lockwood et al. (2000) and Wild et al. (2001) have estimated the spatial extent of FTEs and found their observed FTEs span >4 h in local time. McWilliams et al. (2000b) observed that the source of FTEs, i.e., the region of active reconnection, shifts azimuthally over time. Fear et al. (2017) estimated the magnetic flux transferred by individual FTEs to be tens of MWb, which is ∼10% of the flux over the entire polar cap.

PMAFs are not only related to the reconnection at the magnetopause but also to the plasma convection pattern as can be determined from radar measurements (Tremsina et al. 2017). The IMF B_y can shift the convection pattern asymmetrically towards dawn or dusk and will thus determine the direction of motion of PMAFs. Part of the asymmetry between PMAFs during northward and southward IMF B_z may arise from the difficulty in distinguishing PMAFs and other type of auroral emissions with a north-south drift.

A number of in-situ measurements have provided important information about PMAFs, their evolution and effects. Oksavik et al. (2005) used a wide range of ground- and space-based data, including three low-altitude polar-orbiting spacecraft, to highlight a train of narrow flow channels drifting into the polar cap, related to a PMAF event. Lorentzen et al. (2010) used data from the Investigation of Cusp Irregularities 2 rocket to show that PMAFs continuously evolve to patches.

The Sounding of the Cusp Ion Fountain Energization Region (SCIFER) sounding rocket reached an apogee of nearly 1500 km. Kintner et al. (1996) (also see Arnoldy et al. 1996b and Lorentzen et al. 1996) provide an abundance of data explaining the physics of ionospheric plasma fountain formation in association with a PMAF. Related work is provided by Lund et al. (2012), who used SCIFER2 data to show electron heating signatures at altitudes of nearly 1500 km, above PMAF activity below.

The Rocket Experiment for Neutral Upwelling 2 (RENU2) rocket was launched on Dec 13, 2015 at 07:34 UT (Lessard et al. 2019). The solar wind speed averaged 520 km/s with B_z 1.5 nT and B_y 3.5 nT, producing the desired PMAF activity. The payload reached its apogee of 447 km as it crossed over Svalbard. Data acquired during the flight include electron distribution functions (Kenward et al. 2019), ion distribution functions and upflow/downflow (Godbole et al. 2019), neutral populations (Clemmons et al. 2019; Fritz et al. 2019) and photometers (Hecht et al. 2019), as well as electric and magnetic fields and a comprehensive set of ground instrumentation.

RENU2 data highlight two important processes. One has to do with the basic PMAF structure. Although in a typical keogram, PMAF activity appears as the poleward motion of a broad, isolated arc, RENU2 observations show that this aurora actually consists of clusters of highly-dynamic, multiple thin arcs, near 100 m in thickness, driven by soft electron precipitation (Kenward et al. 2019). With an apparent poleward motion that is faster than measured convection speeds, the implication is that the passage of a sequence of PMAFs delivers a series of transient, quasi-periodic energy fluxes to any given flux tube.

In addition, timescales for electron, ion and neutral particle dynamics range from a few seconds to tens of minutes. Timescales between PMAF passages are typically less than the time required to heat the neutral particles (10 min) (Carlson et al. 2012). Therefore, each

PMAF encounters a region having an initial condition that includes the recent history of the region—that is, hysteresis in the system is important. Perhaps more importantly, the differences in timescales tend to drive altitudinal and latitudinal neutral density structuring, including up to altitudes near 500 km or higher.

Although PMAFs gradually fade as they propagate away from the cusp, the magnetic flux tube continues to propagate into the polar cap. Chapter (XX paper on polar cap patches of this volume XX) describes more details on how PMAFs connect to polar cap patches and nightside auroral activity.

5.5 TCV Aurora

Traveling Convection Vortices (TCVs) are ionospheric structures having vortical flows around pairs of field-aligned currents in opposite hemispheres, typically taken to be signatures of dayside reconnection that propagate anti-sunward at high-latitudes. Murr et al. (2002) describe typical properties of TCVs, noting that "they form near noon at latitudes typically near 73° magnetic latitude and propagate antisunward with velocities of 5–10 km/s. They have scale sizes of 1000–3000 km and are observed most frequently a few hours prenoon and postnoon with the majority of events observed in the prenoon sector."

Initial studies of TCVs and related phenomena attempted to understand ground-based magnetometer signatures associated with a so-called flux transfer event (or FTE, which had been identified as evidence for sporadic reconnection on the dayside Russell and Elphic 1978; Berchem and Russell 1984), Lanzerotti et al. (1986) present observations showing two such events, but without explicitly calling them TCVs. The basis for event identification in that study included the use of a simple model showing the expected topology and ground magnetometer signatures as described by Lee and Fu (1985).

Interhemispheric FTE signatures were considered by Lanzerotti et al. (1990), who examined magnetic field data acquired at high-latitude, near-conjugate stations and identified numerous events that could be interpreted as having signatures of field-aligned currents above the stations. These authors introduced the term "Magnetic Impulse Events" (MIE) for these events. Related work by Friis-Christensen et al. (1988) also examined magnetometer signatures of such events, though these authors used the term "Traveling Convection Vortices" (TCVs), which has become the more common term.

Auroral observations associated with TCVs (or MIEs) have been observed in 630.0 and 427.8 nm all-sky images (Mende et al. 1990, 2001; Kataoka et al. 2001), though with the 630.0 emission line being dominant. A typical example of ground-based observations of a TCV aurora event is given in Fig. 9 from Kim et al. (2017b). Weatherwax et al. (1999) showed riometer signatures associated with 427.8 nm emissions. Murr et al. (2002) also reported a 427.8 nm auroral arc, extending ∼600 km in length. Kataoka et al. (2003) reported transient enhancements in UV auroral intensity, extending ∼500 km in length and width, related to the passage of a TCV current system in POLAR-UVI images. Finally, Ebihara et al. (2008) report observations of proton aurora during TCVs, typically ∼300–500 km in length and ∼150–200 km in width that lasted for ∼1–2 minutes.

A signature of proton aurora is consistent with various observations of ion cyclotron waves occurring with TCVs (Arnoldy et al. 1996a; Sakaguchi et al. 2007; Yahnin et al. 2007; Yahnina et al. 2008), where the waves may have precipitated the protons. Engebretson et al. (2013) showed evidence of ion cyclotron wave signatures in the ground during a TCV that transited Svalbard. The waves were associated with proton precipitation and were deemed to have been generated on closed field lines (see, also, Posch et al. 2013 and Kim et al. 2017a).

Finally, coupling of the vortical to the thermosphere has been shown for one TCV event, over Svalbard by Kim et al. (2017b), who also show ion cyclotron wave occurrences at the
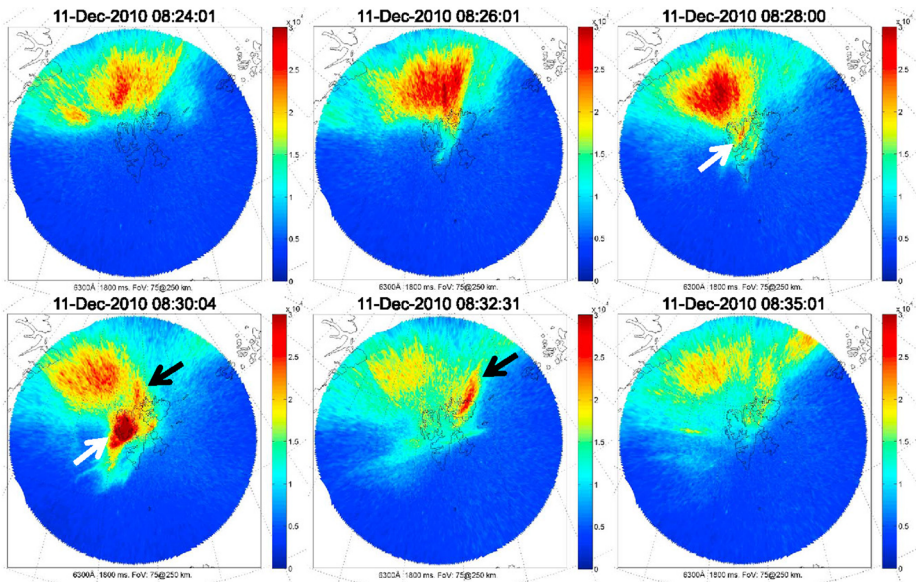
Fig. 9 All-sky camera images at 630.0 nm acquired during a TCV event. The emissions occurring poleward of the station before the event are thought to be cusp precipitation. The emissions associated with the TCVs are the brief, bright spots. Adapted from Kim et al. (2017b)

approximate time of the TCV arrival, implying that they were generated by a temperature anisotropy resulting from a compression on the dayside magnetosphere. The possible mechanisms to cause the magnetopause compression include localized pressure pulses (Glassmeier and Heppner 1992), hot flow anomalies (Sitar et al. 1998; Sibeck et al. 1999), and foreshock cavities (Murr and Hughes 2003).

5.6 Throat Aurora

Throat aurora is a particular auroral form observed around the dayside ionospheric convection throat region, which was first defined during an extensive study on dayside diffuse aurora (Han et al. 2015). Throat auroras typically exhibit as north-south aligned discrete auroral forms extending from the equatorward edge of the east-west-aligned auroral oval toward low latitude as shown in Fig. 10. The main observational properties of throat aurora have been investigated (Han et al. 2015, 2016, 2017a, 2018; Chen et al. 2017). It has been confirmed that throat auroras are caused by precipitation of particles originated from the magnetosheath (Han et al. 2016). Recently, Han et al. (2018) provide apparent one-to-one correspondences between throat auroras observed on the ground and magnetopause transients observed by MMS satellites near the subsolar magnetopause, which have been suggested to be the direct evidence for throat auroras being the ionospheric signature of magnetopause indentations. In addition, it was found that the spatial scale of the magnetopause indentation can be as large as $\sim 2.0 \times 3.0$ R_e after mapping a throat aurora to the geomagnetic equatorial plane, and the daily occurrence rate is higher than $\sim 50\%$ (Han et al. 2017a). These observational results indicate that throat aurora may reflect an important process that commonly occurs on the subsolar magnetopause.

On considering how the throat auroras are generated, Han et al. (2017a) pointed out that stripy diffuse aurora connecting to the discrete aurora oval seems to be a necessary
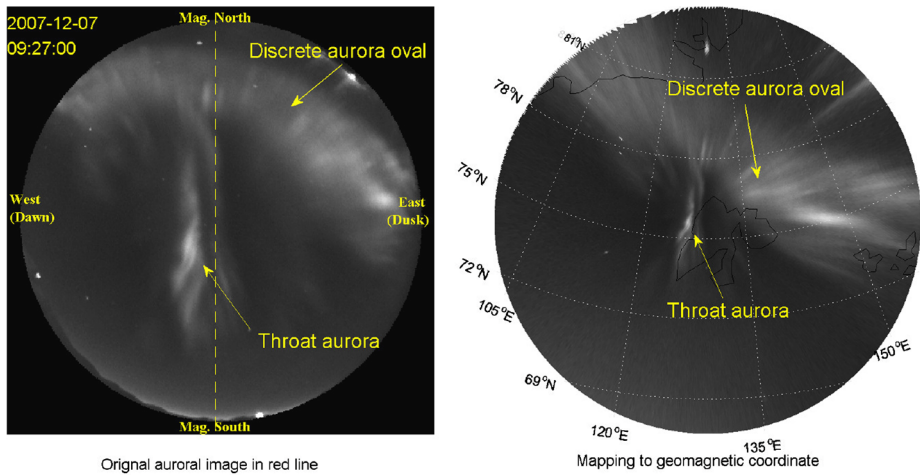
Fig. 10 A typical throat aurora observed at Yellow River Station by all-sky camera on 7 December 2007 shown (left) in original observation and (right) after mapping to geomagnetic coordinates (from Han et al. 2018). According to previous studies (e.g., Lockwood 1997), the equatorward edge of the discrete aurora oval near local noon can be regarded as the open-closed field line boundary

condition for the occurrence of throat aurora. It was also noticed that orientations of throat aurora are convection-aligned (Han et al. 2017a). Because diffuse auroras are caused by precipitation of particles from the central plasma sheet that is inside the magnetosphere and the convection is also a magnetosphere internal process, these observational results indicate that the occurrence of throat aurora is affected by factors from inside the magnetosphere. At the same time, Han et al. (2017a) found that the occurrence rate of throat aurora shows a clear dependence on the IMF cone angle ($arccos[|B_x|/B_{total}]$). This suggests that some outside factors, such as magnetosheath high-speed jets, might be a driver for producing the throat auroras (Han et al. 2017a; Plaschke et al. 2018). It is puzzling why the generation of throat aurora depends on factors either inside or outside of the magnetosphere.

Recently, Han (2019) proposed a conceptual model for throat aurora. The model suggests that precipitation of a stripy diffuse aurora can lead to ionospheric conductivity enhancement and thus produce a polarization electric field in the ionosphere. This electric field maps to the magnetopause along closed field lines, and may affect the magnetopause reconnection to develop an inward motion and result in a throat aurora. This model can explain why the occurrence of throat aurora depends on either inside or outside factors, because it has been confirmed that two types of diffuse aurora exist near magnetic local noon, which are related with inside and outside factors, respectively (Han et al. 2017b). Furthermore, using coordinated observations from THEMIS and all-sky camera observations at South Pole station, Wang et al. (2018a) showed that magnetosheath high-speed jets were well associated the localized diffuse auroral brightening observed at South Pole station near local noon. This provides support to the model of Han (2019). According to this model, the outside factors may not drive throat aurora directly, but produce diffuse aurora first, change the ionospheric conductivity, set up a polarization electric field, and some feedback could then affect the magnetopause reconnection and result in throat aurora. Some observational support for the model was presented in Han (2019).

Very recent results provide evidence for throat aurora being associated with magnetopause reconnection (Han et al. 2019). Throat auroras have been suggested to be related

to indentations on the subsolar magnetopause. However, the indentation generation process and the resulting ionospheric responses have remained unknown. An EISCAT Svalbard Radar experiment enabled the authors for the first time to observe the temporal and spatial evolution of flow reversals, Joule heating, and ion upflows associated with throat aurora. The high-resolution data allowed to discriminate that the flow bursts and Joule heating were concurrent and co-located, but were always observed on the west side of the associated throat auroras, reflecting that the upward/downward field-aligned currents associated with throat aurora are always to the east/west, respectively. These results are consistent with the geometry of the flux transfer event model (Southwood 1987) and provide strong evidence for throat aurora being associated with magnetopause reconnection.

6 Shock Aurora

Shock aurora is a subset of dayside aurora associated with the sudden enhancements of solar wind dynamic pressure that occurs at an interplanetary shock. The processes responsible for the shock aurora are complicated, as the Interplanetary Magnetic Field (IMF) is also highly variable. Consequently, some of the signatures of shock aurora are associated with changes in the reconnection topology. Indeed Zhou et al. (2017) list four different processes that could generate shock aurora. These are:

1. Enhanced pitch angle diffusion associated with direct compression of the magnetospheric magnetic field (Zhou and Tsurutani 1999; Zhou et al. 2003, 2009);
2. Fast mode (compressional) waves launched by the shock and propagating through the magnetosphere, generating traveling convection vortices (TVCs) and the associated field-aligned currents that generate aurora (Zhou et al. 2010; Zhang et al. 2002);
3. Alfvén waves launched through magnetic reconnection, with these waves supporting parallel electric fields, and hence particle acceleration through kinetic effects, i.e., electron thermal pressure (Chaston et al. 2005; Zhou et al. 2009) and
4. Flow and magnetic field shears that generate field-aligned currents that in turn require parallel electrostatic potentials, much like the discrete aurora on the nightside.

We note that many of these processes are discussed in other sections of this chapter, and indeed many of the processes are not unique to shock aurora. Haerendel (2011), in discussing different auroral generators, includes both Alfvén wave generated aurora (process 3 above) and quasi-static potentials (process 4). In this Chapter TCVs are discussed in Sect. 5.5 as a consequence of reconnection imposed flows, while Sect. 7 discusses diffuse aurora and the association with pitch angle scattering. The difference here is that there is a direct association of the arrival of an interplanetary shock and the resultant aurora.

The most directly shock-related aurora is that associated with enhanced wave-induced particle precipitation. As discussed by Zhou and Tsurutani (1999) and Zhou et al. (2017), the effect of the shock-induced magnetic field compression is to enhance the perpendicular energy of the near equatorial particle distribution in the magnetosphere. This in turn results in wave instabilities that isotropize the distribution, increasing the energy flux in the loss cone. This in turn leads to diffuse aurora.

Fast-mode wave-related TCVs are also primarily associated with solar wind dynamic pressure enhancements. In this case the fast-mode waves convert to shear-mode waves, as these are the only waves that carry field-aligned current. This allows the vortical flow around the fast-mode wave to be transmitted to the ionosphere. As with nightside aurora, the associated field-aligned currents could have energetic (100 eV to several keV) electron

precipitation associated with them either through quasi-static electric fields (Knight 1973), or through Alfvén waves (Chaston et al. 2005). In the latter case the Alfvén waves can carry a field-aligned electric field through either kinetic (electron pressure) or inertial (electron inertia) effects (see Lysak and Song 2003 for a discussion of how non-ideal-MHD Alfvén waves can have a parallel electric field associated with them).

Simultaneous observations of the electron and proton aurora during a solar wind pressure pulse showed the slightly different behavior to the shock arrival (Meurant et al. 2003). It was found that the electron and the proton precipitation both start in the post noon sector and expand concurrently, but the expansion into the nightside starts sooner for the protons than for the electrons. In situ electron measurements in the afternoon sector indicate that the shock has a significant effect on the electron spectral characteristics. It is suggested that the various Alfvén frequencies generated by the shock account for the two different speeds of propagation of the disturbance. Other observations showed that the propagation from the noon to the night sector mainly occurs through the afternoon region for proton precipitation and the morning sector for electron aurora, as expected from the azimuthal drift of newly injected plasma (Meurant et al. 2004). The asymmetry of the precipitation distribution around the noon-midnight axis is more pronounced during negative B_z periods, when activity is the most important. It was suggested that adiabatic compression and plasma waves play an important role on the locations of electron and proton precipitation in the dayside. It was also shown that some shocks are able to trigger substorms when they hit an unstable magnetosphere (Meurant et al. 2005).

Figure 11 shows the complexity of the various processes associated with shock aurora and the resultant precipitating electron signatures. The left hand side of the figure shows an electron energy-time spectrogram as the FAST spacecraft passes from low to high latitudes, leaving the plasma-sheet (as evidenced by several keV electrons) into the polar cap. For this pass the spacecraft passes through a region of intense moderate energy ($<$500 eV) electrons. Magnetometer data (not shown) show highly variable FAC structure throughout this region. The right-hand side of the figure shows a 2-D phase space density contour plot for the time indicated by the vertical white line in the left-hand panel. The distribution, which has been clipped at 10^{-10} s^3 cm^{-3} km^{-3}, shows a clear loss-cone on the left-hand side. These particles, with speeds $>10^4$ km/s ($>$300 eV), are mainly of magnetosheath origin, although they may have been further energized by waves at higher altitudes. The lower energy electrons show bi-directional fluxes. This is indicative of local wave acceleration.
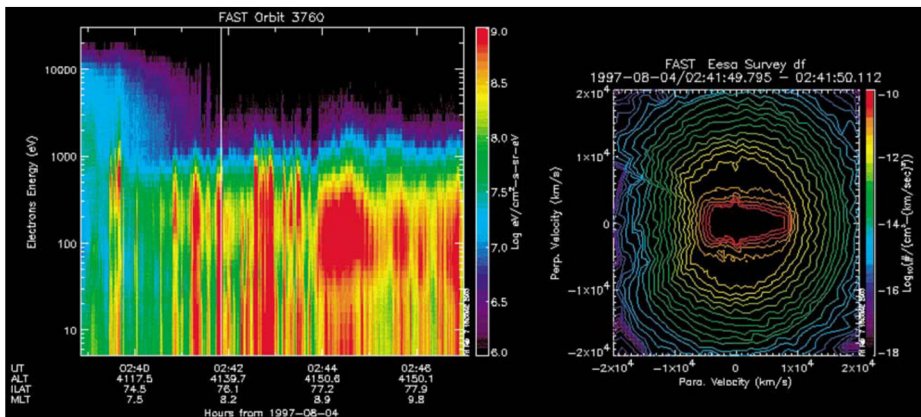

Fig. 11 Example of shock aurora observed by the FAST spacecraft (after Zhou et al. 2009)

In summary, shock aurora is a highly complex phenomenon. Some of the signatures are directly attributable to the shock passage (diffuse aurora from wave-induced precipitation, TCVs from compressional fast-mode waves), while others are reminiscent of processes associated with nightside aurora, but in this case connected to the dayside magnetopause, through either reconnection or boundary layer motion through Kelvin-Helmholtz waves. The shock aurora in this case is either directly related to FACs, or parallel acceleration by kinetic or inertial Alfvén waves.
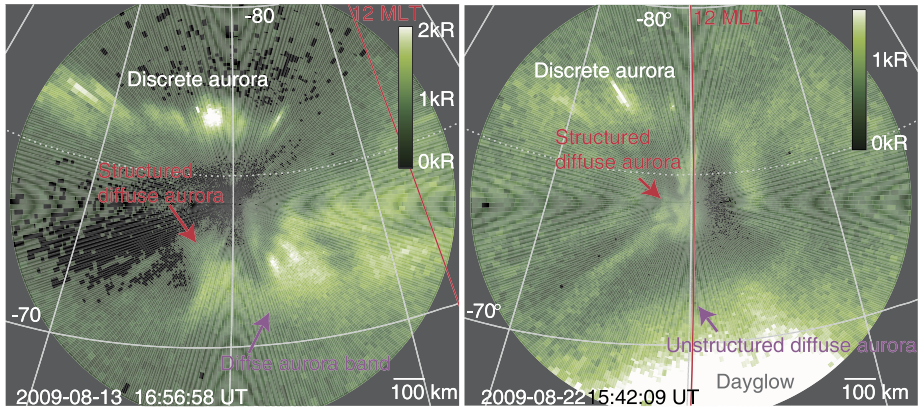
7 Dayside Diffuse Aurora

The equatorward portion of the dayside auroral oval is dominated by diffuse aurora including pulsating aurora (Lorentzen et al. 1996; Sandholt et al. 2002b). The spectral intensity is primarily at the 557.7 nm wavelength ($I_{630.0}/I_{557.7} < 1$), and the emission is driven by precipitating electrons of a few keV energy scattered by waves in the dayside plasma sheet through wave-particle interaction. Ni et al. (2016) provide an extensive review of the wave-particle interaction and driving processes of diffuse auroral precipitation.

Dayside diffuse aurora is more intense at pre-noon than post-noon, and is a common structure particularly at magnetically quiet times, although it is more intense at active times (Newell et al. 2009; Han et al. 2015). This is consistent with the fact that whistler-mode waves in the magnetosphere occur more frequently on the dayside than nightside even with low amplitudes (Li et al. 2011) and that plasma sheet electron fluxes are higher at pre-noon because electron populations decrease as they experience magnetic drifts from the nightside through dawn.

Despite the diffuse appearance, a variety of structures can be found in the diffuse auroral region:

1. Pulsating aurora occurs in the poleward portion of the diffuse aurora region and is associated with energy-dispersed electron precipitation (Lorentzen et al. 1996). Dayside pulsating aurora intensifies by extending from the nightside during substorms (Royrvik and Davis 1977).
2. Particularly near noon, the diffuse aurora shows patches, bands, stripes and irregular forms of some tens of km size. Examples are shown in Fig. 12. The diffuse auroral structures drift at the large-scale convection speed, and diffuse auroral stripes are suggested to occur in the dayside convection throat (Ebihara et al. 2007; Han et al. 2015). Some of them have been shown to connect to nearly north-south aligned discrete aurora called throat aurora (Han et al. 2016) (see Sect. 5.6).
3. Faster propagation of patches beyond convection speed (~20 km/s) has also been found, in association with Pc3 ULF pulsations (Motoba et al. 2017).
4. Black aurora is also embedded in the structure-less diffuse auroral background (Han et al. 2015).

Satellite-ground conjugate observations have shown that the diffuse auroral patches correspond to low-energy (<~50 eV) plasma density structures in the dayside outer magnetosphere at $L > {\sim}6$ R_e (Nishimura et al. 2013). Whistler-mode waves are intensified in the high-density regions, while plasma sheet electrons of >1 keV do not show similar structures (Nishimura et al. 2013). Growth rates of whistler-mode waves are enhanced in the high-density regions due to lower resonant energy, and the waves increase pitch angle scattering of plasma sheet electrons into the loss cone. This process explains the formation of the localized patches of diffuse aurora and is consistent with the motion of patches being at

Fig. 12 Examples of dayside diffuse aurora. Diffuse aurora occurs equatorward of discrete aurora and shows different types of structures (Nishimura et al. 2013)

large-scale convection speed rather than magnetic drift speed of energetic electrons. Numerical calculations have also demonstrated that enhanced waves can drive sufficient electron precipitation flux for the measured level of diffuse auroral intensity (Ni et al. 2014).

Dayside diffuse aurora also shows rapid temporal variations. Solar wind dynamic pressure enhancements associated with interplanetary shocks create abrupt intensifications of diffuse aurora due to large-scale magnetosphere compression (Zhou et al. 2003; Nishimura et al. 2016) (see also Sect. 6). Recently, diffuse aurora has also been found to brighten associated with IMF discontinuities, some of which create compressions and rarefactions through interaction with the bow shock (foreshock transients). The 2D structure and propagation of diffuse auroral features were able to reveal a few R_e azimuthal size of localized compression and its azimuthal propagation at ∼100 km/s (Wang et al. 2018b). Dayside diffuse aurora also present localized modulation without appreciable changes in the solar wind. Those are particularly seen under B_x-dominant IMF, where magnetosheath high-speed jets (HSJs) are created and compress the magnetopause locally (a few R_e azimuthal size) (Wang et al. 2018a).

8 Morning Side Diffuse Aurora Spots

A most likely diffuse spot of aurora was often seen in X-ray images by the Polar spacecraft PIXIE instrument (Imhof et al. 1995), while it was not seen in better spatial resolution observations by Polar-UVI (Torr et al. 1995) or VIS (Frank et al. 1995). The "traditional" UV aurora instruments UVI and VIS are sensitive to emissions that are generated by precipitating electrons up to ≈25 keV, PIXIE was specifically sensitive to emissions from high energy electrons (>10 keV). Delayed about 30 minutes relative to substorm onsets, a localized maximum of X-ray emission was observed at 5–9 hours magnetic local time (Østgaard et al. 1999) where no corresponding UV emissions were seen (Fig. 13). By identifying the location of the injection region and determining the substorm onset time it was speculated that this maximum most probably is caused by electrons injected in the midnight sector and then drifting (i.e., gradient and curvature drift) into a region in the dawnside magnetosphere where some mechanism effectively scatters the electrons into the loss cone. Later more de-

Panel G 1430 - 1440 UT

Panel G 1434:07 UT
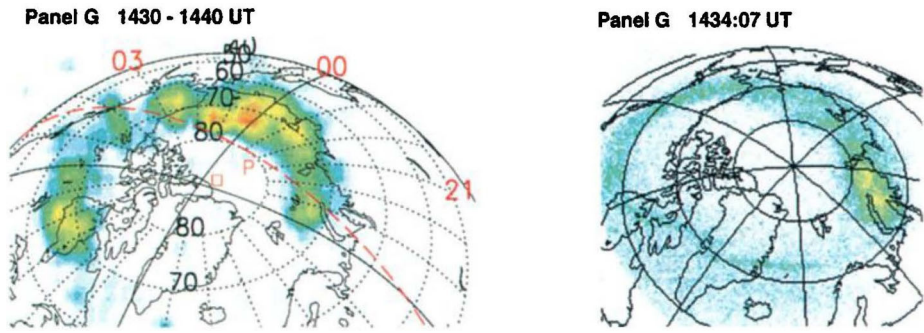
Fig. 13 Example of a diffuse morning side spot emission in X-rays (left) but nothing is seen in UV emissions (right). Adapted from Østgaard et al. (1999)

tailed investigations including ground-based and in situ measurements from high- and low-altitude satellites provided more information about the global characteristics of such events (Østgaard et al. 2000a). It could be confirmed that the time delay between substorm onset around midnight and the appearance of the spots on the morning side is similar to the drift time of energetic electrons. The electron spectra measured in the early stage of the localized morning maximum of X-ray emission strongly indicate that the scattering of >2–10 keV electrons by wave-particle interaction into the loss cone is the main mechanism for this precipitation (Østgaard et al. 2000b). Such high energy electrons (up to 200 keV) have already been found in this general local time region much earlier (McDiarmid et al. 1975). It was also found that a high energy ($\approx$30–100 keV) component of the precipitating electron population contributes $\approx$30% of the total electron energy flux in that region (Cummer et al. 2000).

9 Conclusions

Most dayside aurora phenomena are driven by reconnection between the solar wind and the terrestrial magnetic field at the dayside magnetopause. Studying dayside aurora can thus provide a lot of insight into the solar wind–magnetosphere interaction. This review summarizes the properties, dynamics, and driving solar wind conditions for dayside aurora phenomena. Even though past space missions and ground-based observations have provided a lot of information about these processes there are still a number of open questions. For instance, what is the time scale between the arrival of solar wind structures at the magnetopause and the visible response in the dayside aurora dynamics or appearance? Is there a quantitative relationship between the magnitude and orientation of the IMF and the response in dayside auroral forms? Why do PMAFs occur during northward and southward IMF? Does steady or pulsed reconnection display a similar temporal behavior in cusp aurora brightness and appearance? Can we infer lobe reconnection properties from observations of HiLDA? Can the extent of the reconnection X-line be inferred from PMAF observations? Is the proposed model for throat aurora correct or does need to be adjusted with more detailed observations? Why does shock aurora appear to be related to the shock passage and dayside processes but also to nightside processes? Unfortunately, there are no immediate plans for the launch of satellites that could provide long-term and continuous observations of dayside aurora and we can only hope that in-situ measurements and model calculations with appropriate inputs will enhance our knowledge about dayside aurora and the interactions at the magnetopause.

Publisher's Note   Springer Nature remains neutral with regard to jurisdictional claims in published maps and institutional affiliations.

References

G.A. Abel, M.P. Freeman, A statistical analysis of ionospheric velocity and magnetic field power spectra at the time of pulsed ionospheric flows. J. Geophys. Res. **107**, 1470 (2002). https://doi.org/10.1029/2002JA009402

R.L. Arnoldy, M.J. Engebretson, J.L. Alford, R.E. Erlandson, B.J. Anderson, Magnetic impulse events and associated Pc 1 bursts at dayside high latitudes. J. Geophys. Res. **101**, 7793 (1996a). https://doi.org/10.1029/95JA03378

R.L. Arnoldy, K.A. Lynch, P.M. Kintner, J. Bonnell, T.E. Moore, C.J. Pollock, SCIFER—Structure of the Cleft Ion Fountain at 1400 km altitude. Geophys. Res. Lett. **23**, 1869–1872 (1996b). https://doi.org/10.1029/96GL00475

J. Berchem, C.T. Russell, Flux transfer events on the magnetopause—spatial distribution and controlling factors. J. Geophys. Res. **89**, 6689 (1984). https://doi.org/10.1029/JA089iA08p06689

H.C. Carlson, Sharpening our thinking about polar cap ionospheric patch morphology, research, and mitigation techniques. Radio Sci. **47**, RS0L21 (2012). https://doi.org/10.1029/2011RS004946

H.C. Carlson, T. Spain, A. Aruliah, A. Skjaeveland, J. Moen, First principles physics of cusp/polar cap thermospheric disturbances. Geophys. Res. Lett. **39**, L19103 (2012). https://doi.org/10.1029/2012GL053034

J.A. Carter, S.E. Milan, A.R. Fogg, L.J. Paxton, B.J. Anderson, The association of high-latitude dayside aurora with NBZ field-aligned currents. J. Geophys. Res. (2018). https://doi.org/10.1029/2017JA025082

C.C. Chaston, L.M. Peticolas, C.W. Carlson, J.P. McFadden, F. Mozer, M. Wilber, G.K. Parks, A. Hull, R.E. Ergun, R.J. Strangeway, M. Andre, Y. Khotyaintsev, M.L. Goldstein, M. Acuna, E.J. Lund, H. Reme, I. Dandouras, A.N. Fazakerley, A. Balogh, Energy deposition by Alfvén waves into the dayside auroral oval: Cluster and FAST observations. J. Geophys. Res. **110**, A02211 (2005). https://doi.org/10.1029/2004JA010483

X.C. Chen, D.S. Han, D.A. Lorentzen, K. Oksavik, J.I. Moen, L.J. Baddeley, Dynamic properties of throat aurora revealed by simultaneous ground and satellite observations. J. Geophys. Res. **122**, 3469–3486 (2017). https://doi.org/10.1002/2016JA023033

G. Chisham, M. Lester, S.E. Milan, M.P. Freeman, W.A. Bristow, A. Grocott, K.A. McWilliams, J.M. Ruohoniemi, T.K. Yeoman, P.L. Dyson, R.A. Greenwald, T. Kikuchi, M. Pinnock, J.P.S. Rash, N. Sato, G.J. Sofko, J.-P. Villain, A.D.M. Walker, A decade of the Super Dual Auroral Radar Net-work (SuperDARN): scientific achievements, new techniques and future directions. Surv. Geophys. **28**, 33–109 (2007). https://doi.org/10.1007/s10712-007-9017-8

J.H. Clemmons, R.L. Walterscheid, D.G. Brinkman, J.H. Hecht, M.R. Lessard, B.A. Fritz, D.R. Kenward, L.B.N. Clausen, D.L. Hysell, The neutral atmosphere during the RENU2 investigation. Geophys. Res. Lett. (2019, submitted)

I.J. Coleman, G. Chisham, M. Pinnock, M.P. Freeman, An ionospheric convection signature of antiparallel reconnection. J. Geophys. Res. **106**, 28,995–29,007 (2001)

B.M.A. Cooling, C.J. Owen, S.J. Schwartz, Role of the magnetosheath flow in determining the motion of open flux tubes. J. Geophys. Res. **106**, 18,763–18,776 (2001)

S.W.H. Cowley, M. Lockwood, Excitation and decay of solar wind-driven flows in the magnetosphere-ionosphere system. Ann. Geophys. **10**, 103–115 (1992)

S.A. Cummer, R.R. Vondrak, N. Østgaard, J. Stadsnes, J. Bjordal, D.L. Chenette, M.J. Brittnacher, G.K. Parks, J.B. Sigwarth, L.A. Frank, Global multispectral auroral imaging of an isolated substorm. Geophys. Res. Lett. **27**, 637–640 (2000). https://doi.org/10.1029/1999GL003678

J.A. Davies, T.K. Yeoman, I.J. Rae, S.E. Milan, M. Lester, M. Lockwood, A. McWilliams, Ground-based observations of the auroral zone and polar cap ionospheric responses to dayside transient reconnection. Ann. Geophys. **20**, 781–794 (2000). https://doi.org/10.5194/angeo-20-781-2002

E.E. Drury, S.B. Mende, H.U. Frey, J.H. Doolittle, Southern Hemisphere poleward moving auroral forms. J. Geophys. Res. **108**, 1114 (2003). https://doi.org/10.1029/2001JA007536

Y. Ebihara, Y.M. Tanaka, S. Takasaki, A.T. Weatherwax, M. Taguchi, Quasi-stationary auroral patches observed at the South Pole Station. J. Geophys. Res. **112**, A01201 (2007). https://doi.org/10.1029/2006JA012087

Y. Ebihara, R. Kataoka, A.T. Weatherwax, M. Yamauchi, J. Geophys. Res. **113**, A07209 (2008). https://doi.org/10.1029/2008JA013099

M.J. Engebretson et al., Multi-instrument observations from Svalbard of a traveling convection vortex, electromagnetic ion cyclotron wave burst, and proton precipitation associated with a bow shock instability. J. Geophys. Res. **118**, 2975 (2013). https://doi.org/10.1002/jgra.50291

C.J. Farrugia, R.P. Rijnbeek, M.A. Saunders, D.J. Southwood, D.J. Rodgers, M.F. Smith, L.J.C. Woolliscroft, A multi-instrument study of flux transfer event structure. J. Geophys. Res. **93**, 14,465–14,477 (1988). https://doi.org/10.1029/JA093iA12p14465

C.J. Farrugia et al., Pulsed flows at the high-altitude cusp poleward boundary, and associated ionospheric convection and particle signatures, during a Cluster–FAST–SuperDARN- Søndrestrøm conjunction under a southwest IMF. Ann. Geophys. **22**, 2891–2905 (2004). https://doi.org/10.5194/angeo-22-2891-2004

G.J. Fasel, Dayside poleward moving auroral forms: a statistical study. J. Geophys. Res. **100**(A7), 11891–11905 (1995). https://doi.org/10.1029/95JA00854

G.J. Fasel, L.C. Lee, R.W. Smith, A mechanism for the multiple brightenings of dayside poleward-moving auroral forms. Geophys. Res. Lett. **20**(20), 2247–2250 (1993). https://doi.org/10.1029/93GL02487

R.C. Fear et al., Motion of flux transfer events: a test of the Cooling model. Ann. Geophys. **25**, 1669–1690 (2007). www.ann-geophys.net/25/1669/2007/

R.C. Fear, L. Trenchi, J.C. Coxon, S.E. Milan, How much flux does a flux transfer event transfer? J. Geophys. Res. **122**, 12,310–12,327 (2017). https://doi.org/10.1002/2017JA024730

Y.I. Feldstein, Auroral oval. J. Geophys. Res. **78**, 1210 (1973)

L.A. Frank, J.B. Sigwarth, J.D. Craven, J.P. Cravens, J.S. Dolan, M.R. Dvorsky, P.K. Hardebeck, J.D. Harvey, D.W. Muller, The Visible Imaging System (VIS) for the polar spacecraft. Space Sci. Rev. **71**, 297–328 (1995). https://doi.org/10.1007/BF00751334

H.U. Frey, Localized aurora beyond the auroral oval. Rev. Geophys. **45** (2007). https://doi.org/10.1029/2005RG000174

H.U. Frey, S.B. Mende, T.J. Immel, S.A. Fuselier, E.S. Claflin, J.-C. Gérard, B. Hubert, Proton aurora in the cusp. J. Geophys. Res. **107**, 1091 (2002). https://doi.org/10.1029/2001JA900161

H.U. Frey, T.J. Immel, G. Lu, J. Bonnell, S.A. Fuselier, S.B. Mende, B. Hubert, N. Østgaard, G. Le, Properties of localized, high latitude, dayside aurora. J. Geophys. Res. **108**, 8008 (2003a). https://doi.org/10.1029/2002JA009332

H.U. Frey, S.B. Mende, S.A. Fuselier, T.J. Immel, N. Østgaard, Proton aurora in the cusp during southward IMF. J. Geophys. Res. **108**, 1277 (2003b). https://doi.org/10.1029/2003JA009861

H.U. Frey, T.D. Phan, S.A. Fuselier, S.B. Mende, Continuous magnetic reconnection at Earth's magnetopause. Nature **426**, 533–537 (2003c)

H.U. Frey, N. Østgaard, T.J. Immel, H. Korth, S.B. Mende, Seasonal dependence of localized, High Latitude Dayside Aurora (HiLDA). J. Geophys. Res. **109**, A04303 (2004). https://doi.org/10.1029/2003JA010293

E. Friis-Christensen, M.A. McHenry, C.R. Clauer, S. Vennerstrøm, Ionospheric traveling convection vortices observed near the polar cleft—a triggered response to sudden changes in the solar wind. Geophys. Res. Lett. **15**, 253 (1988). https://doi.org/10.1029/GL015i003p00253

B.A. Fritz, M.R. Lessard, K.F. Dymond, D.L. Kenward, K.A. Lynch, J.H. Hecht, J.H. Clemmons, RENU2 UV PMT observations in the cusp. Geophys. Res. Lett. (2019). https://doi.org/10.1029/2019GL082314

S.A. Fuselier, H.U. Frey, K.J. Trattner, S.B. Mende, J.L. Burch, Cusp aurora dependence on IMF B_z. J. Geophys. Res. **107** (2002). https://doi.org/10.1029/2001JA900165

S.A. Fuselier, S.B. Mende, T.E. Moore, H.U. Frey, S.B. Petrinec, E.S. Claflin, M.R. Collier, Cusp dynamics and ionospheric outflow. Space Sci. Rev. **109**, 285–312 (2003). https://doi.org/10.1023/B:SPAC.0000007522.71147.b3

S.A. Fuselier, K.J. Trattner, S.M. Petrinec, Antiparallel and component reconnection at the dayside magnetopause. J. Geophys. Res. **116**, A10227 (2011). https://doi.org/10.1029/2011JA016888

K.-H. Glassmeier, C. Heppner, Traveling magnetospheric convection twin vortices: another case study, global characteristics, and a model. J. Geophys. Res. **97**(A4), 3977 (1992). https://doi.org/10.1029/91JA02464

K.H. Glassmeier, M. Stellmacher, Mapping flux transfer events to the ionosphere. Adv. Space Res. **18**(8), 151 (1996)

N.H. Godbole et al., RENU2 observations of ion upflow and downflow. Geophys. Res. Lett. (2019, submitted)

G. Haerendel, Six auroral generators: a review. J. Geophys. Res. **116**, A00K05 (2011). https://doi.org/10.1029/2010JA016425. Printed **117**(A1) (2012)

G. Haerendel, G. Paschmann, N. Sckopke, H. Rosenbauer, P.C. Hedgecock, The frontside boundary layer of the magnetosphere and the problem of reconnection. J. Geophys. Res. **83**(A7), 3195 (1978). https://doi.org/10.1029/JA083iA07p03195

D.S. Han, Ionospheric polarization electric field guiding magnetopause reconnection: a conceptual model of throat aurora. Sci. China Earth Sci. **62** (2019). https://doi.org/10.1007/s11430-019-9358-8

D. Han, X.-C. Chen, J.-J. Liu, Q. Qiu, K. Keika, Z.-J. Hu, J.-M. Liu, H.-Q. Hu, H.-G. Yang, An extensive survey of dayside diffuse aurora based on optical observations at Yellow River Station. J. Geophys. Res. **120**(9), 7447 (2015). https://doi.org/10.1002/2015ja021699

D.S. Han, Y. Nishimura, L.R. Lyons, H.Q. Hu, H.G. Yang, Throat aurora: the ionospheric signature of magnetosheath particles penetrating into the magnetosphere. Geophys. Res. Lett. **43**, 1819–1827 (2016). https://doi.org/10.1002/2016GL068181

D.S. Han, H. Hietala, X.C. Chen, Y. Nishimura, L.R. Lyons, J.J. Liu, H.Q. Hu, H.G. Yang, Observational properties of dayside throat aurora and implications on the possible generation mechanisms. J. Geophys. Res. **122**, 1853 (2017a). https://doi.org/10.1002/2016ja023394

D.S. Han, J.-X. Li et al., Coordinated observations of two types of diffuse auroras near magnetic local noon by Magnetospheric Multiscale mission and ground all-sky camera. Geophys. Res. Lett. **44**(16), 8130 (2017b). https://doi.org/10.1002/2017gl074447

D.-S. Han, J.J. Liu, X.C. Chen, T. Xu, B. Li, Z.J. Hu, H.Q. Hu, H.G. Yang, S.A. Fuselier, C.J. Pollock, Direct evidence for throat aurora being the ionospheric signature of magnetopause transient and reflecting localized magnetopause indentations. J. Geophys. Res. (2018). https://doi.org/10.1002/2017ja024945

D.S. Han, T. Xu, Y. Jin, K. Oksavik, X.C. Chen, J.J. Liu et al., Observational evidence for throat aurora being associated with magnetopause reconnection. Geophys. Res. Lett. **46**, 7113–7120 (2019). https://doi.org/10.1029/2019GL083593

J.H. Hecht, J.H. Clemmons, M.R. Lessard, D.L. Kenward, B.F. Sadler, B.A. Fritz, J.S. Evans, K.A. Lynch, A new technique for estimating the lifetime of bursts of electron precipitation from sounding rocket measurementsb. Geophys. Res. Lett. (2019). https://doi.org/10.1029/2019GL082894

J.L. Horwitz, S.I. Akasofu, The response of the dayside aurora to sharp northward and southward transitions of the interplanetary magnetic field and to magnetospheric substorms. J. Geophys. Res. **82**(19), 2723 (1977). https://doi.org/10.1029/JA082i019p02723

S.M. Imber, S.E. Milan, B. Hubert, Ionospheric flow and auroral signatures of dual lobe re-connection. Ann. Geophys. **24**, 3115–3129 (2006)

W.L. Imhof, K.A. Spear, J.W. Hamilton, B.R. Higgins, M.J. Murphy, J.G. Pronko, R.R. Vondrak, D.L. McKenzie, C.J. Rice, D.J. Gorney, D.A. Roux, R.L. Williams, J.A. Stein, J. Bjordal, J. Stadsnes, K. Njoten, T.J. Rosenberg, L. Lutz, D. Detrick, The Polar Ionospheric X-Ray Imaging Experiment (PIXIE). Space Sci. Rev. **71**, 385–408 (1995). https://doi.org/10.1007/BF00751336

M.G. Johnsen, D.A. Lorentzen, A statistical analysis of the optical dayside open/closed field line boundary. J. Geophys. Res. **117**, A02218 (2012). https://doi.org/10.1029/2011JA016984

R. Kataoka, H. Fukunishi, L.J. Lanzerotti, C.G. Maclennan, H.U. Frey, S.B. Mende, J.H. Doolittle, T.J. Rosenberg, A.T. Weatherwax, Magnetic impulse event: a detailed case study of extended ground and space observations. J. Geophys. Res. **106**(A11), 25873 (2001). https://doi.org/10.1029/2000JA000314

R. Kataoka, H. Fukunishi, K. Hosokawa, H. Fujiwara, A.S. Yukimatu, N. Sato, Y.-K. Tung, Transient production of F-region irregularities associated with TCV passage. Ann. Geophys. **21**, 1531 (2003). https://doi.org/10.5194/angeo-21-1531-2003

D.L. Kenward, M.R. Lessard, B.A. Fritz, I.J. Cohen, Characterization of soft electron precipitation in the cusp region during poleward moving auroral form event. Geophys. Res. Lett. (2019, submitted)

H. Kim et al., Conjugate observations of electromagnetic ion cyclotron waves associated with traveling convection vortex events. J. Geophys. Res. **122**, 7336 (2017a). https://doi.org/10.1002/2017JA024108

H. Kim et al., Simultaneous observations of traveling convection vortices: ionosphere-thermosphere coupling. J. Geophys. Res. **122**, 4943 (2017b). https://doi.org/10.1002/2017JA023904

P.M. Kintner et al., The SCIFER experiment. Geophys. Res. Lett. **23**, 1865 (1996). https://doi.org/10.1029/96GL01260

S. Knight, Parallel electric fields. Planet. Space Sci. **21**, 741–750 (1973)

J. Kuijpers, H.U. Frey, L. Fletcher, Electric current circuits in astrophysics. Space Sci. Rev. **188**, 3–57 (2015). https://doi.org/10.1007/s11214-014-0041-y

L.J. Lanzerotti, L.C. Lee, C.G. Maclennan, A. Wolfe, L.V. Medford, Possible evidence of flux transfer events in the polar ionosphere. Geophys. Res. Lett. **13**, 1089 (1986). https://doi.org/10.1029/GL013i011p01089

L.J. Lanzerotti, A. Wolfe, N. Trivedi, C.G. Maclennan, L.V. Medford, Magnetic impulse events at high latitudes—magnetopause and boundary layer plasma processes. J. Geophys. Res. **95**, 97 (1990). https://doi.org/10.1029/JA095iA01p00097

L.C. Lee, Z.F. Fu, A theory of magnetic flux transfer at the Earth's magnetopause. Geophys. Res. Lett. **12**, 105 (1985). https://doi.org/10.1029/GL012i002p00105

M.R. Lessard et al., Overview of the Rocket Experiment for Neutral Upwelling sounding Rocket 2 (RENU2). Geophys. Res. Lett. (2019). https://doi.org/10.1029/2018GL081885

W. Li, J. Bortnik, R.M. Thorne, V. Angelopoulos, Global distribution of wave amplitudes and wave normal angles of chorus waves using THEMIS wave observations. J. Geophys. Res. **116**, A12205 (2011). https://doi.org/10.1029/2011JA017035

M. Lockwood, Relationship of dayside auroral precipitations to the open-closed separatrix and the pattern of convective flow. J. Geophys. Res. **102**(17), 17,475–17,487 (1997)

M. Lockwood, Identifying the open-closed field line boundary, in *Polar Cap Boundary Phenomena*, ed. by J. Moen, A. Egeland, M. Lockwood. NATO ASI Series, vol. 509 (Kluwer Academic Publishers, Dordrecht, 1998), pp. 73–90

M. Lockwood, S.W.H. Cowley, P.E. Sandholt, R.P. Lepping, The ionospheric signatures of flux transfer events and solar wind dynamic pressure changes. J. Geophys. Res. **95**, 17,113 (1990). https://doi.org/10.1029/JA095iA10p17113

M. Lockwood, H.C. Carlson, P.E. Sandholt, The implications of the altitude of transient 630 nm dayside auroral emission. J. Geophys. Res. **98**, 15,571–15,587 (1993)

M. Lockwood, S.W.H. Cowley, M.F. Smith, R.P. Rijnbeek, R.C. Elphic, The contribution of flux transfer events to convection. Geophys. Res. Lett. **22**, 1185–1188 (1995)

M. Lockwood, C.J. Davis, T.G. Onsager, J.A. Scudder, Modelling signatures of pulsed magnetopause reconnection in cusp ion dispersion signatures seen at middle altitudes. Geophys. Res. Lett. **25**, 591–594 (1998)

M. Lockwood, I.W. McCrea, S.E. Milan, J. Moen, J.C. Cerisier, A. Thorolfsson, Plasma structure within poleward-moving cusp-cleft auroral transients: EISCAT Svalbard radar observations and an explanation in terms of large local time extent of events. Ann. Geophys. **18**, 1027 (2000)

M. Lockwood, S.E. Milan, T. Onsager, C.H. Perry, J.A. Scudder, C.T. Russell, M. Brittnacher, Cusp ion steps, field-aligned currents and poleward moving auroral forms. J. Geophys. Res. **106**, 29,555–29,569 (2001a)

M. Lockwood, H. Opgenoorth et al., Coordinated Cluster, ground-based instrumentation and low-altitude satellite observations of transient poleward-moving events in the ionosphere and in the tail lobe. Ann. Geophys. **19**, 1589–1612 (2001b). https://doi.org/10.5194/angeo-19-1589-2001

D.A. Lorentzen, C.S. Deehr, J.I. Minow, R.W. Smith, H.C. Stenbaek-Nielsen, F. Sigernes, SCIFER-dayside auroral signatures of magnetospheric energetic electrons. Geophys. Res. Lett. **23**, 1885 (1996). https://doi.org/10.1029/96GL00593

D.A. Lorentzen, J. Moen, K. Oksavik, F. Sigernes, Y. Saito, M.G. Johnsen, In situ measurement of a newly created polar cap patch. J. Geophys. Res. **115**, A12323 (2010). https://doi.org/10.1029/2010JA015710

E.J. Lund et al., Electron temperature in the cusp as measured with the SCIFER-2 sounding rocket. J. Geophys. Res. **117**, A06326 (2012). https://doi.org/10.1029/2011JA017404

R.L. Lysak, Y. Song, Kinetic theory of the Alfvén wave acceleration of auroral electrons. J. Geophys. Res. **108**(A4), 8005 (2003). https://doi.org/10.1029/2002JA009406

A. Marchaudon, J.-C. Cerisier, J.-M. Bosqued, M.W. Dunlop, J.A. Wild, P.M.E. Decreau, M. Forster, D. Fontaine, H. Laakso, Transient plasma injections in the dayside magnetosphere: one-to-one correlated observations by Cluster and SuperDARN. Ann. Geophys. **22**, 141–158 (2004). https://doi.org/10.5194/angeo-22-141-2004

N.C. Maynard et al., Characteristics of merging at the magnetopause inferred from dayside 557.7 nm all-sky images: IMF drivers of poleward moving auroral forms. Ann. Geophys. **24**, 3071 (2006). https://doi.org/10.5194/angeo-24-3071-2006

I.B. McDiarmid, J.R. Burrows, E.E. Budzinski, Average characteristics of magnetospheric electrons (140 eV to 200 keV) at 1400 kilometers. J. Geophys. Res. **80**, 73–79 (1975)

K.A. McWilliams, T.K. Yeoman, S.W.H. Cowley, Two-dimensional electric field measurements in the ionospheric footprint of a flux transfer event. Ann. Geophys. **18**, 1584–1598 (2000a). https://doi.org/10.1007/s00585-001-1584-2

K.A. McWilliams, T.K. Yeoman, G. Provan, A statistical survey of dayside pulsed ionospheric flows as seen by the CUTLASS Finland HF radar. Ann. Geophys. **18**, 445–453 (2000b). https://doi.org/10.1007/s00585-000-0445-8

S.B. Mende, R.L. Rairden, L.J. Lanzerotti, C.G. Maclennan, Magnetic impulses and associated optical signatures in the dayside aurora. Geophys. Res. Lett. **17**, 131 (1990). https://doi.org/10.1029/GL017i002p00131

S.B. Mende, H.U. Frey, J.H. Doolittle, L. Lanzerotti, C.G. Maclennan, Dayside optical and magnetic correlation events. J. Geophys. Res. **106**, 24637 (2001). https://doi.org/10.1029/2001JA900065

S.B. Mende, H.U. Frey, J. McFadden, C.W. Carlson, V. Angelopoulos, K.H. Glassmeier, D.G. Sibeck, A. Weatherwax, Coordinated observation of the dayside magnetospheric entry and exit of the THEMIS satellites with ground-based auroral imaging in Antarctica. J. Geophys. Res. **114**, A00C23 (2009). https://doi.org/10.1029/2008JA013496

M. Meurant, J.-C. Gerard, B. Hubert, V. Coumans, C. Blockx, N. Østgaard, S.B. Mende, Dynamics of global scale electron and proton precipitation induced by a solar wind pressure pulse. Geophys. Res. Lett. **30**, 2032 (2003). https://doi.org/10.1029/2003GL018017

M. Meurant, J.-C. Gerard, C. Blockx, B. Hubert, V. Coumans, Propagation of electron and proton shock-induced aurora and the role of the interplanetary magnetic field and solar wind. J. Geophys. Res. **109**, A10210 (2004). https://doi.org/10.1029/2004JA010453

M. Meurant, J.-C. Gerard, C. Blockx, V. Coumans, B. Hubert, M. Connors, L.R. Lyons, E. Donovan, Comparison of intense nightside shock-induced precipitation and substorm activity. J. Geophys. Res. **110**, A07228 (2005). https://doi.org/10.1029/2004JA010916

S.E. Milan, M. Lester, S.W.H. Cowley, J. Moen, P.E. Sandholt, C.J. Owen, Meridian-scanning photometer, coherent HF radar, and magnetometer observations of the cusp: a case study. Ann. Geophys. **17**, 159–172 (1999a)

S.E. Milan, T.K. Yeoman, M. Lester, J. Moen, P.E. Sandholt, Post-noon two-minute period pulsating aurora and their relationship to the dayside convection pattern. Ann. Geophys. **17**(7), 877 (1999b). https://doi.org/10.1007/s00585-999-0877-8

S.E. Milan, M. Lester, S.W.H. Cowley, M. Brittnacher, Convection and auroral response to a southward turning of the IMF: polar UVI, CUTLASS, and IMAGE signatures of transient magnetic flux transfer at the magnetopause. J. Geophys. Res. **105**(A7), 15741 (2000a). https://doi.org/10.1029/2000JA900022

S.E. Milan, M. Lester, S.W.H. Cowley, M. Brittnacher, Dayside convection and auroral morphology during an interval of northward interplanetary magnetic field. Ann. Geophys. **18**, 436–444 (2000b)

S.E. Milan, M. Lester, S.W.H. Cowley, K. Oksavik, M. Brittnacher, R.A. Greenwald, G. Sofko, J.-P. Villain, Variations in polar cap area during two substorm cycles. Ann. Geophys. **21**, 1121–1140 (2003)

S.E. Milan, G. Provan, B. Hubert, Magnetic flux transport in the Dungey cycle: a survey of dayside and nightside reconnection rates. J. Geophys. Res. **112**, A01209 (2007). https://doi.org/10.1029/2006JA011642

S.E. Milan, S.M. Imber, J.A. Carter, M.T. Walach, B. Hubert, What controls the local time extent of flux transfer events? J. Geophys. Res. **121**, 1391 (2016). https://doi.org/10.1002/2015JA022012

S.E. Milan, L.B.N. Clausen, J.C. Coxon, J.A. Carter, M.-T. Walach, K. Laundal, N. Østgaard, P. Tenfjord, J. Reistad, K. Snekvik, H. Korth, B.J. Anderson, Overview of solar wind-magnetosphere-ionosphere-atmosphere coupling and the generation of magnetospheric currents. Space Sci. Rev. **206**, 547–573 (2017). https://doi.org/10.1007/s11214-017-0333-0

J. Moen, Y. Rinne, H.C. Carlson, K. Oksavik, R. Fujii, H. Opgenoorth, On the relationship between thin Birkeland current arcs and reversed flow channels in the winter cusp/cleft ionosphere. J. Geophys. Res. **113**, A09220 (2008). https://doi.org/10.1029/2008JA013061

J. Moen, H. Carlson, Y. Rinne, A. Skjaeveland, Multi-scale features of solar terrestrial coupling in the cusp ionosphere. J. Atmos. Sol.-Terr. Phys. **87**, 11 (2012). https://doi.org/10.1016/j.jastp.2011.07.002

T. Motoba, Y. Ebihara, A. Kadokura, M.J. Engebretson, M.R. Lessard, A.T. Weatherwax, A.J. Gerrard, Fast-moving diffuse auroral patches: a new aspect of daytime Pc3 auroral pulsations. J. Geophys. Res. **122**, 1542 (2017). https://doi.org/10.1002/2016JA023285

D.L. Murr, W.J. Hughes, Solar wind drivers of Traveling Convection Vortices. Geophys. Res. Lett. **30**(7), 1354 (2003). https://doi.org/10.1029/2002GL015498

D.L. Murr, W.J. Hughes, A.S. Rodger, E. Zesta, H.U. Frey, A.T. Weatherwax, Conjugate observations of traveling convection vortices: the field-aligned current system. J. Geophys. Res. **107**, 1306 (2002). https://doi.org/10.1029/2002JA009456

D.A. Neudegg et al., A survey of magnetopause FTEs and associated flow bursts in the polar ionosphere. Ann. Geophys. **18**, 416–435 (2000). https://doi.org/10.1007/s00585-000-0416-0

D.A. Neudegg et al., The UV aurora and ionospheric flows during flux transfer events. Ann. Geophys. **19**, 179–188 (2001). https://doi.org/10.5194/angeo-19-179-2001

P.T. Newell, C.-I. Meng, Ion acceleration at the equatorward edge of the cusp: low altitude observations of patchy merging. Geophys. Res. Lett. **18**, 1829–1832 (1991)

P.T. Newell, J.M. Ruohoniemi, C.-I. Meng, Maps of precipitation by source region, binned by IMF, with inertial convection streamlines. J. Geophys. Res. **109**, A10206 (2004). https://doi.org/10.1029/2004JA010499

P.T. Newell, S. Wing, C.I. Meng, Spectral properties and source regions of dayside electron acceleration events. J. Geophys. Res. **110**, A11205 (2005). https://doi.org/10.1029/2005JA011264

P.T. Newell, T. Sotirelis, K. Liou, C.-I. Meng, F.J. Rich, Cusp latitude and the optimal solar wind coupling function. J. Geophys. Res. **111**, A09207 (2006). https://doi.org/10.1029/2006JA011731

P.T. Newell, T. Sotirelis, S. Wing, Diffuse, monoenergetic, and broadband aurora: the global precipitation budget. J. Geophys. Res. **114**, A09207 (2009). https://doi.org/10.1029/2009JA014326

B. Ni, J. Bortnik, Y. Nishimura, R.M. Thorne, W. Li, V. Angelopoulos, Chorus wave scattering responsible for the Earth's dayside diffuse auroral precipitation: a detailed case study. J. Geophys. Res. **119**, 897 (2014). https://doi.org/10.1002/2013JA019507

B. Ni, R.M. Thorne, X. Zhang, J. Bortnik, Z. Pu, L. Xie, Origins of the Earth's diffuse auroral precipitation. Space Sci. Rev. **200**, 205 (2016). https://doi.org/10.1007/s11214-016-0234-7

Y. Nishimura, J. Bortnik, W. Li, R.M. Thorne, B. Ni, L.R. Lyons, Structures of dayside whistler-mode waves deduced from conjugate diffuse aurora. J. Geophys. Res. **118**, 664 (2013). https://doi.org/10.1029/2012JA018242

Y. Nishimura, T. Kikuchi, Y. Ebihara, A. Yoshikawa, S. Imajo, W. Li, H. Utada, Evolution of the current system during solar wind pressure pulses based on aurora and magnetometer observations. Earth Planets Space **68**(1), 144 (2016)

K. Oksavik, J. Moen, H.C. Carlson, High-resolution observations of the small-scale flow pattern associated with a poleward moving auroral form in the cusp. Geophys. Res. Lett. **31**, L11807 (2004). https://doi.org/10.1029/2005GL019838

K. Oksavik, J. Moen, H.C. Carlson, R.A. Greenwald, S.E. Milan, M. Lester, R.J. Barnes, Multi-instrument mapping of the small-scale flow dynamics related to a cusp auroral transient. Ann. Geophys. **23**, 2657 (2005)

N. Østgaard, J. Stadsnes, J. Bjordal, R.R. Vondrak, S.A. Cummer, D.L. Chenette, G.K. Parks, M.J. Brittnacher, D.L. McKenzie, Global-scale electron precipitation features seen in UV and X rays during substorms. J. Geophys. Res. **104**, 10191–10204 (1999). https://doi.org/10.1029/1999JA900004

N. Østgaard, J. Stadsnes, J. Bjordal, G.A. Germany, R.R. Vondrak, G.K. Parks, S.A. Cummer, D.L. Chenette, J.G. Pronko, Auroral electron distributions derived from combined UV and X-ray emissions. J. Geophys. Res. **106**, 26081–26090 (2000a). https://doi.org/10.1029/2001JA000031

N. Østgaard, J. Stadsnes, J. Bjordal, R.R. Vondrak, S.A. Cummer, D.L. Chenette, M. Schulz, J.G. Pronko, Cause of the localized maximum of X-ray emission in the morning sector: a comparison with electron measurements. J. Geophys. Res. **105**, 20869–20884 (2000b). https://doi.org/10.1029/1999JA000354

N. Østgaard, S.B. Mende, H.U. Frey, J.B. Sigwarth, Simultaneous imaging of the reconnection spot in the opposite hemispheres during northward IMF. Geophys. Res. Lett. **32**, L21104 (2005). https://doi.org/10.1029/2005GL024491

N. Østgaard et al., The asymmetric geospace as displayed during the geomagnetic storm on 17 August 2001. Ann. Geophys. **36**, 1577 (2018). https://doi.org/10.5194/angeo-36-1577-2018

G. Paschmann, G. Haerendel, I. Papamastorakis, N. Sckopke, S.J. Bame, J.T. Gosling, C.T. Russell, Plasma and magnetic field characteristics of magnetic flux transfer events. J. Geophys. Res. **87**, 2159 (1982). https://doi.org/10.1029/JA087iA04p02159

T.D. Phan et al., Simultaneous Cluster and IMAGE observations of cusp reconnection and auroral proton spot for northward IMF. Geophys. Res. Lett. **30**(10), 1509 (2003). https://doi.org/10.1029/2003GL016885

F. Plaschke, H. Hietala, M. Archer, X. Blanco-Cano, P. Kajdic, T. Karlsson, H.L. Sun, N. Omidi, M. Palmroth, V. Roytershteyn, Jets downstream of collisionless shocks. Space Sci. Rev. **214**(5), 81 (2018)

J.L. Posch, M.J. Engebretson, A.J. Witte, D.L. Murr, M.R. Lessard, M.G. Johnsen, H.J. Singer, M.D. Hartinger, Simultaneous traveling convection vortex events and Pc1 wave bursts at cusp latitudes observed in Arctic Canada and Svalbard. J. Geophys. Res. Space Phys. **118**, 6352 (2013). https://doi.org/10.1002/jgra.50604

P. Prikryl, G. Provan, K.A. McWilliams, T.K. Yeoman, Ionospheric cusp flows pulsed by solar wind Alfvén waves. Ann. Geophys. **20**, 161–174 (2002). https://doi.org/10.5194/angeo-20-161-2002

G. Provan, T.K. Yeoman, Statistical observations of the MLT, latitude and size of pulsed ionospheric flows with the CUTLASS Finland radar. Ann. Geophys. **17**, 855–867 (1999). https://doi.org/10.1007/s00585-999-0855-1

G. Provan, T.K. Yeoman, S.W.H. Cowley, The influence of the IMF B_y component on the locations of pulsed flows in the dayside ionosphere as observed by HF radar. Geophys. Res. Lett. **26**, 521 (1999)

G. Provan, M. Lester, A. Grocott, S.W.H. Cowley, Pulsed flows observed during an interval of prolonged northward IMF. Ann. Geophys. **23**, 1207–1225 (2005). https://doi.org/10.5194/angeo-23-1207-2005

M.I. Pudovkin, S.A. Zaitseva, P.E. Sandholt, A. Egeland, Dynamics of aurorae in the cusp region and characteristics of magnetic reconnection at the magnetopause. Planet. Space Sci. **40**, 879 (1992)

I.J. Rae, F.R. Fenrich, M. Lester, K.A. McWilliams, J.D. Scudder, Solar wind modulation of cusp particle signatures and their associated ionospheric flows. J. Geophys. Res. **109**, A03223, 10/1029/2003JA010188 (2004)

P.H. Reiff, T.W. Hill, J.L. Burch, Solar wind plasma injection at the dayside magnetospheric cusp. J. Geophys. Res. **82**, 479–487 (1977)

Y. Rinne, J. Moen, K. Oksavik, H.C. Carlson, Reversed flow events in the winter cusp ionosphere observed by the European Incoherent Scatter (EISCAT) Svalbard radar. J. Geophys. Res. **112**, A10313 (2007). https://doi.org/10.1029/2007JA012366

O. Royrvik, T.N. Davis, Pulsating aurora: local and global morphology. J. Geophys. Res. **82**(29), 4720 (1977). https://doi.org/10.1029/JA082i029p04720

C.T. Russell, R.C. Elphic, Initial ISEE magnetometer results—magnetopause observations. Space Sci. Rev. **22**, 681 (1978). https://doi.org/10.1007/BF00212619

C.T. Russell, R.C. Elphic, ISEE observations of flux transfer events at the dayside magnetopause. Geophys. Res. Lett. **6**, 33 (1979). https://doi.org/10.1029/GL006i001p00033

K. Sakaguchi, K. Shiokawa, A. Ieda, Y. Miyoshi, T. Otsuka, T. Ogawa, M. Connors, E.F. Donovan, F.J. Rich, Simultaneous ground and satellite observations of an isolated proton arc at subauroral latitudes. J. Geophys. Res. **112**, A04202 (2007). https://doi.org/10.1029/2006JA012135

P.E. Sandholt, C.J. Farrugia, Monitoring magnetosheath-magnetosphere interconnection topography from the aurora. Ann. Geophys. **20**, 629 (2002)

P.E. Sandholt, P.T. Newell, Ground and satellite observations of an auroral event at the cusp/cleft equatorward boundary. J. Geophys. Res. **97**(A6), 8685 (1992). https://doi.org/10.1029/91JA02995

P.E. Sandholt, C.S. Deehr, A. Egeland, B. Lybekk, R. Viereck, G.J. Romick, Signatures in the dayside aurora of plasma transfer from the magnetosheath. J. Geophys. Res. **91**(A9), 10063 (1986). https://doi.org/10.1029/JA091iA09p10063

P.E. Sandholt, H.C. Carlson, A. Egeland, *Dayside and Polar Cap Aurora*. Astrophysics and Space Science Library, vol. 270 (Kluwer Academic Publishers, Dordrecht/Boston/London, 2002a)

P.E. Sandholt, W.F. Denig, C.J. Farrugia, B. Lybekk, E. Trondsen, Auroral structure at the cusp equatorward boundary: relationship with the electron edge of low-latitude boundary layer precipitation. J. Geophys. Res. **107**(A9), 1235 (2002b). https://doi.org/10.1029/2001JA005081

P.E. Sandholt, C.J. Farrugia, W.F. Denig, S.W.H. Cowley, M. Lester, Spontaneous and driven cusp dynamics: optical aurora, particle precipitation, and plasma convection. Planet. Space Sci. **51**(12), 797 (2003a). https://doi.org/10.1016/S0032-0633(03)00114-4

P.E. Sandholt, J. Moen, C.J. Farrugia, S.W.H. Cowley, M. Lester, S.E. Milan, C. Valladares, W.F. Denig, S. Eriksson, Multi-site observations of the association between aurora and plasma convection in the cusp/polar cap during a southeastward ($B_y \sim \|B_z\|$) IMF orientation. Ann. Geophys. **21**, 539 (2003b). https://doi.org/10.5194/angeo-21-539-2003

P.E. Sandholt, C.J. Farrugia, W.F. Denig, Dayside aurora and the role of IMF $|B_y/B_z|$: detailed morphology and response to magnetopause reconnection. Ann. Geophys. **22**, 613 (2004). https://doi.org/10.5194/angeo-22-613-2004

D.G. Sibeck et al., Comprehensive study of the magnetospheric response to a hot flow anomaly. J. Geophys. Res. **104**(A3), 4577 (1999). https://doi.org/10.1029/1998JA900021

R.J. Sitar, J.B. Baker, C.R. Clauer, A.J. Ridley, J.A. Cumnock, V.O. Papitashvili, J. Spann, M.J. Brittnacher, G.K. Parks, Multi-instrument analysis of the ionospheric signatures of a hot flow anomaly occurring on July 24, 1996. J. Geophys. Res. **103**(A10), 23357 (1998). https://doi.org/10.1029/98JA01916

A. Skjaveland, J. Moen, H.C. Carlson, On the relationship between flux transfer events, temperature enhancements, and ion upflow events in the cusp ionosphere. J. Geophys. Res. **116**, A10305 (2011). https://doi.org/10.1029/2011JA016480

D.J. Southwood, The ionospheric signature of flux transfer events. J. Geophys. Res. **92**(A4), 3207 (1987). https://doi.org/10.1029/JA092iA04p03207

A. Thorolfsson, J.C. Cerisier, M. Lockwood, P.E. Sandholt, C. Senior, M. Lester, Simultaneous optical and radar signatures of poleward moving auroral forms. Ann. Geophys. **18**, 1054 (2000). https://doi.org/10.1007/s00585-000-1054-2

M.R. Torr, D.G. Torr, M. Zukic, R.B. Johnson, J. Ajello, P. Banks, K. Clark, K. Cole, C. Keffer, G. Parks, B. Tsurutani, J. Spann, A far ultraviolet imager for the International Solar-Terrestrial Physics Mission. Space Sci. Rev. **71**, 329 (1995). https://doi.org/10.1007/BF00751335

K.J. Trattner, S.A. Fuselier, W.K. Peterson, M. Boehm, D. Klumpar, C.W. Carlson, T.K. Yeoman, Temporal versus spatial interpretation of cusp ion structures observed by two spacecraft. J. Geophys. Res. **107**(A10), 1287 (2002). https://doi.org/10.1029/2001JA000181

E.A. Tremsina, S.B. Mende, H.U. Frey, Identifying the evolution of Southern Hemisphere poleward moving auroral forms (PMAFs) in the context of plasma convection and magnetic reconnection. J. Geophys. Res. Space Phys. **122**, 4037–4050 (2017). https://doi.org/10.1002/2016JA023426

V.G. Vorobjev, G. Gustafsson, G.V. Starkov, Y.I. Feldstein, N.F. Shevnina, Dynamics of day and night aurora during substorms. Planet. Space Sci. **23**, 269 (1975). https://doi.org/10.1016/0032-0633(75)90132-4

B. Wang, Y. Nishimura, L.R. Lyons, Y. Zou, H.C. Carlson, H.U. Frey, S.B. Mende, Analysis of close conjunctions between dayside polar cap airglow patches and flow channels by all-sky imager and DMSP. Earth Planets Space **68**(1), 150 (2016a). https://doi.org/10.1186/s40623-016-0524-z

B. Wang, Y. Nishimura, Y. Zou, L.R. Lyons, V. Angelopoulos, H. Frey, S. Mende, Investigation of triggering of poleward moving auroral forms using satellite-imager coordinated observations. J. Geophys. Res. **121**, 10,929 (2016b). https://doi.org/10.1002/2016JA023128

B. Wang, Y. Nishimura, H. Hietala, L. Lyons, V. Angelopoulos, F. Plaschke, Impacts of magnetosheath high-speed jets on the magnetosphere and ionosphere measured by optical imaging and satellite observations. J. Geophys. Res. **123**, 4879 (2018a). https://doi.org/10.1029/2017JA024954

B. Wang, Y. Nishimura, H. Hietala, X.C. Shen, Q. Shi, H. Zhang, Dayside magnetospheric and ionospheric responses to a foreshock transient on June 25, 2008: 2.2-D evolution based on dayside auroral imaging. J. Geophys. Res. **123**, 6347 (2018b). https://doi.org/10.1029/2017JA024846

A.T. Weatherwax, H.B. Vo, T.J. Rosenberg, S.B. Mende, H.U. Frey, L.J. Lanzerotti, C.G. Maclennan, A dayside ionospheric absorption perturbation in response to a large deformation of the magnetopause. Geophys. Res. Lett. **26**, 517 (1999). https://doi.org/10.1029/1999GL900017

J.A. Wild et al., First simultaneous observations of flux transfer events at the high-latitude magnetopause by the Cluster spacecraft and pulsed radar signatures in the conjugate ionosphere by the CUTLASS and EISCAT radars. Ann. Geophys. **19**, 1491–1508 (2001). https://doi.org/10.5194/angeo-19-1491-2001

J.A. Wild, S.E. Milan, S.W.H. Cowley, M.W. Dunlop, C.J. Owen, J.M. Bosqued, H. Reme, Coordinated interhemispheric SuperDARN radar observations of the ionospheric response to flux transfer events observed by the Cluster spacecraft at the high-latitude magnetopause. Ann. Geophys. **21**, 1807 (2003). https://doi.org/10.5194/angeo-21-1807-2003

S. Wing, P.T. Newell, C.-I. Meng, Cusp modeling and observations at low latitude. Surv. Geophys. **26**, 341–367 (2005). https://doi.org/10.1007/s10712-005-1886-0

J. Woch, R. Lundin, Magnetosheath plasma precipitation in the polar cusp and its control by the interplanetary magnetic field. J. Geophys. Res. **97**, 1421–1430 (1992)

Z.Y. Xing et al., Poleward moving auroral forms (PMAFs) observed at the Yellow River Station: a statistical study of its dependence on the solar wind conditions. J. Atmos. Sol.-Terr. Phys. **86**, 25 (2012). https://doi.org/10.1016/j.astp.2012.06.004

A.G. Yahnin, T.A. Yahnina, H.U. Frey, Subauroral proton spots visualize the Pc1 source. J. Geophys. Res. **112**, A10223 (2007). https://doi.org/10.1029/2007JA012501

T.A. Yahnina, H.U. Frey, T. Bösinger, A.G. Yahnin, Evidence for subauroral proton flashes on the dayside as the result of the ion cyclotron interaction. J. Geophys. Res. **113**, A07209 (2008). https://doi.org/10.1029/2008JA013099

T.K. Yeoman, M. Lester, S.W.H. Cowley, S.E. Milan, J. Moen, P.E. Sandholt, Simultaneous observations of the cusp in optical, DMSP and HF radar data. Geophys. Res. Lett. **24**, 2251–2254 (1997)

Y. Zhang, L.J. Paxton, T.J. Immel, H.U. Frey, S.B. Mende, Sudden solar wind dynamic pressure enhancements and dayside detached auroras: IMAGE and DMSP observations. J. Geophys. Res. **108**(A4), 8001 (2002). https://doi.org/10.1029/2002JA009355

Y. Zhang, C.-I. Meng, L.J. Paxton, D. Morrison, B. Wolven, H. Kil, P. Newell, S. Wing, A.B. Christensen, Far-ultraviolet signature of polar cusp during southward IMF B_z observed by TIMED/Global Ultraviolet Imager and DMSP. J. Geophys. Res. **110**, A01218 (2005). https://doi.org/10.1029/2004JA010707

Q.H. Zhang et al., Simultaneous observations of reconnection pulses at Cluster and their effects on the cusp aurora observed at the Chinese Yellow River Station. J. Geophys. Res. **115**, A10237 (2010). https://doi.org/10.1029/2010JA015526

X.-Y. Zhou, B.T. Tsurutani, Rapid intensification and propagation of the dayside aurora: large scale interplanetary pressure pulses (fast shocks). Geophys. Res. Lett. **26**, 1097–1100 (1999)

X.Y. Zhou, R.J. Strangeway, P.C. Anderson, D.G. Sibeck, B.T. Tsurutani, G. Haerendel, H.U. Frey, J.K. Arballo, Shock aurora: FAST and DMSP observations. J. Geophys. Res. **108**(A4), 8019 (2003). https://doi.org/10.1029/2002JA009701

X.-Y. Zhou, K. Fukui, H.C. Carlson, J.I. Moen, R.J. Strangeway, Shock aurora: ground-based imager observations. J. Geophys. Res. **114**, A12216 (2009). https://doi.org/10.1029/2009JA014186

X.-Y. Zhou, D.G. Sibeck, O. Amm, J.M. Ruohoniemi, Interplanetary shock generated ionospheric traveling convection vortex near local noon. Adv. Geosci. **21**, 367–378 (2010)

X.-Y. Zhou, G. Haerendel, J.I. Moen, E. Trondsen, L. Clausen, R.J. Strangeway, B. Lybekk, D.A. Lorentzen, Shock aurora: field-aligned discrete structures moving along the dawnside oval. J. Geophys. Res. **122**, 3145–3162 (2017). https://doi.org/10.1002/2016JA022666